Title

A multi-proxy shallow marine record for Mid-to-Late Holocene climate variability, Thera eruptions and cultural change in the Eastern Mediterranean

Authors

Avnaim-Katav, Simona
Almogi-Labin, Ahuva
Schneider-Mor, Aya
et al.

Publication Date

2019

DOI

10.1016/j.quascirev.2018.12.001

Peer reviewed

Quaternary Science Reviews 204 (2019) 133–148

Contents lists available at ScienceDirect

Quaternary Science Reviews

journal homepage: www.elsevier.com/locate/quascirev

A multi-proxy shallow marine record for Mid-to-Late Holocene climate variability, Thera eruptions and cultural change in the Eastern Mediterranean

Simona Avnaim-Katav [a, b, c, *], Ahuva Almogi-Labin [d], Aya Schneider-Mor [d], Onn Crouvi [d], Aaron A. Burke [e], Konstantine V. Kremenetski [a], Glen M. MacDonald [b, c]

[a] Israel Oceanographic and Limnological Research, P.O.B. 8030, Haifa, 3108001, Israel
[b] University of California, Los Angeles, Institute of the Environment and Sustainability, La Kretz Hall, Suite 300, Box 951496, Los Angeles, CA, 90095-1496, USA
[c] University of California, Los Angeles, Department of Geography, 1255 Bunche Hall, Box 951524, Los Angeles, CA, 90095, USA
[d] Geological Survey of Israel, 30 Malkhe Yisrael, Jerusalem, 95501, Israel
[e] University of California, Los Angeles, Department of Near Eastern Languages and Cultures, 382 Humanities Building, Los Angeles, CA, 90095-1511, USA

ARTICLE INFO

Article history:
Received 12 August 2018
Received in revised form
28 November 2018
Accepted 3 December 2018

Keywords:
Mid-to Late Holocene
Southeastern Mediterranean shelf
Paleoclimatology
Benthic foraminifera
Organic geochemistry
Sedimentation
Pollen
Thera eruption

ABSTRACT

The River Nile catchment is considered the major source of nutrient-rich freshwater and sediment draining into the eastern Mediterranean Sea. Thus, exceptional high-resolution record from the Nile Littoral Cell likely traces changes in the Nile outflows related to climatic changes driven by the monsoonal system. This study used multi-proxy analyses combining sedimentological, geochemical and organic stable isotope data along with foraminiferal data in a southeastern Levantine inner shelf sedimentary sequence to understand Mid - to Late Holocene northeast African climate variability. The palynological record is used to reconstruct local scale changes in the regional vegetation related to the Mediterranean climate system. The analyzed records reveal multi-decadal to centennial pacing of paleoceanographic and paleoclimatic changes, with most prominent events recorded at 4.28, ~3.6 and at 2.9 kyr BP.

These transitional periods characterized by simultaneous high $\delta^{15}N$ values and low total organic carbon (TOC) suggest drier climatic conditions, decrease in Nile discharge, leading to lower nutrient supply. A stable and arid climate during Mid-Late Holocene (~4.5–3.6 cal kyr BP) associated with a weaker monsoon system as well as with a weaker Mediterranean climate system is indicated based on high and constant sedimentation rates (~400 cm kyr^{-1}), along with relatively stable values and only occasional weak fluctuations documented in all of the proxies. This climatic pattern is punctuated by a peak in maximum aridity at 4.28 kyr BP evidenced by low TOC value and low arboreal pollen (AP) and *Artemisia*/Chenopodiaceae (A/C) pollen ratios and the sharp decline in the abundance of benthic foraminifera *Cribroelphidium poeyanum* and *Valvulineria bradyana*. This change corresponds with the well-studied 4.2 kyr BP drought event in the Middle East, Mesopotamia and south Asia.

During the late Holocene (~3.6–2.8 cal. Kyr BP) the climate became unstable characterized by shifts between relatively wetter and drier conditions as evident in considerable fluctuations in all proxies. Maximum positive excursions of TOC values, C/N ratio along with high dominance of opportunistic foraminiferal species (e.g., *Ammonia tepida*) indicate northeast African wetter conditions and increased Nile discharge at 3.5, 3.3, 3.2 and 3.0 kyr BP. The distinct and abrupt transition from a stable to an unstable climate regime around 3.6 kyr BP may have been influenced by the Thera volcanic eruption. Thus, the sedimentary record investigated in this study may provide evidence for the impacts of this well-known volcanic eruption not just on the climate regime in the Levant but also on the ancient Near East and Egypt.

* Corresponding author. Israel Oceanographic and Limnological Research, P.O.B. 8030, Haifa, 3108001, Israel.
E-mail address: simonaav@ocean.org.il (S. Avnaim-Katav).

https://doi.org/10.1016/j.quascirev.2018.12.001
0277-3791/

1. Introduction

The southeastern Mediterranean is an ideal location for reconstructions of past climatic changes, due to its unique physical, geographic, and hydrographic configuration. It is a semi-enclosed basin, almost completely engulfed by densely populated regions and therefore it enables us to understand the environmental changes that took place during historic times. Studying past climatic changes in the eastern Mediterranean during the Mid-to Late Holocene is of great importance since these changes would have significantly impacted the evolution of Middle Bronze Age to Iron Age (ca. 1630–850 BCE) communities throughout the region (e.g., Weiss et al., 1993; Cullen et al., 2000; Staubwasser and Weiss, 2006).

Moreover, our study area in the eastern Mediterranean inner shelf is part of the Nile littoral cell that extends from the western part of the Nile Delta to Haifa Bay some 700 km to the northeast (Fig. 1A). Consequently, the main nutrient-rich freshwater and most sediments of the southeastern Mediterranean inner shelf originated from the Nile River (until its damming in 1965), and were distributed along the Nile littoral cell by prevailing counterclockwise surface currents (e.g., Said, 1993; Krom et al., 1999; Zviely et al., 2007). While this hydrographic pattern has been similar over the Holocene (Fontugne et al., 1994), the supply of these sediments and nutrients has varied over time in response to fluctuations in Nile River discharge, mainly due to climatic changes related to the monsoonal climate system (Almogi-Labin et al., 2009; Box et al., 2011).

Several studies on varied marine sedimentary records show that they are key proxies for reconstructing Holocene climate variability (e.g., Rossignol-Strick and Planchais, 1989; Schilman et al., 2001a; Hennekam et al., 2014, 2015; Mojtahid et al., 2015). In these studies, whatever methodological approaches are used, the reliable reconstructions depend on sedimentation rates at different sites, accurate and sufficient radiometric datings in addition to the application of high resolution analyses.

In deeper water, of the SE Mediterranean slope (at 470 and 670 m water depths) sedimentation rates vary between 85 cm kyr^{-1} at the early part of a 3.6 kyr sedimentary record and 130 cm kyr^{-1} at its most recent part (Schilman et al., 2001a). These values are two orders of magnitude higher than rates documented in eastern Mediterranean deep water sedimentary sequences (e.g., Rossignol-Strick, 1983; Fontugne et al., 1994). Yet, one of the best known sedimentary archives from the southeast Levantine Basin, core PS009PC (taken at 552 m water depth, approximately 100 km southwest of Haifa, Israel) is known to have high sedimentation rates, ranging between 12.5 and 104 cm kyr^{-1}, with the lowest values during the Early-to-Mid Holocene and the highest values during the Late Holocene (Hennekam et al., 2014, 2015; Mojtahid et al., 2015). This core was sampled at a high resolution of 0.5 cm ($\leq$40 year per sample) and it thus tracks centennial Nile River outflow variability based on sediment inorganic geochemistry, planktonic foraminiferal data and pollen. This sedimentary archive encompasses and is dominated by the climatic signal of sapropel S1 (a distinct organic-rich sediment layer) deposited during the early to middle Holocene. Sapropel formation in the eastern Mediterranean is closely associated with periods of enhanced Nile River discharge (Rossignol-Strick et al., 1982) representing the most prominent climatic variability in tropical and northeast Africa (e.g., Almogi-Labin et al., 2009; Box et al., 2011; Hennekam et al., 2014).

The marine sedimentary records from the SE Mediterranean slope show that during the mid- and late Holocene, climate was variable, changing to relatively drier conditions, with alternating episodes between wetter and drier conditions (e.g., Schilman et al., 2001a; Hennekam et al., 2014, 2015). This trend is also documented in the central and eastern Mediterranean regions by various independent terrestrial proxies such as speleothem record and Dead Sea levels (e.g., Migowski et al., 2006; Bar-Matthews and Ayalon, 2011).

At shallower marine sedimentary archives along the SE Mediterranean shelf, variable sedimentation rates characterize the Holocene sedimentary records. In Haifa Bay, off the northern Israeli coast, sedimentation rates are in the order of ~100 cm kyr^{-1} in some inner shelf Holocene sequences (Avnaim-Katav et al., 2012), while off the southern and central Israeli coast higher rates (~140 cm kyr^{-1}) occur during the early Holocene (Avital, 2002; Tapiero, 2002; Porat et al., 2003) and lower ones (<60 cm kyr^{-1}) during the late Holocene. Nonetheless, these scarce published studies were based on a limited number of ^{14}C ages and proxies (i.e., foraminifera and sedimentology), relatively lower sampling resolution for the Holocene and were aimed mainly at resolving general Late Quaternary chronostratigraphy and paleoenvironmental reconstructions, yet not climate variations. Thus, the goal of this study is to add an inclusive understanding of Mid - to Late Holocene paleoclimate variability related to Nile River outflow and to local climate regime based on high resolution shallow marine sedimentary record. In order to fill this gap and achieve our goal in this study we use a sediment core (V-4) recovered from the southeastern Levantine shelf. The core is located at shallow water depth in front of the perennial Alexander River. The general reduction in Nile discharge during the middle to late Holocene caused a gradual narrowing of the Nile plume, which then directed by prevailing counterclockwise moving surface currents into the southeast corner of the Levantine basin, leading to increasing sedimentation rates in that area (Hennekam et al., 2015 and references therein), and even more specifically into the inner shelf. This will enable us to benefit from a) expected high sedimentation rates, and b) mainly reflection of changes in the Nile contribution and some terrestrial input from the adjacent land.

The chronological framework for the core is based on a Bayesian age-depth model using Accelerator Mass Spectrometry ^{14}C measurements. Multiproxy indicators were analyzed in order to elucidate the timing of climate change and its effect on paleoceanographic conditions. Among the ten proxies analyzed we used sedimentation rates and grain size data to delineate sources of fluvial sediments and to detect sedimentation variability in the Nile catchment. C/N ratio is used to define sources of organic matter (marine vs. terrestrial). Total organic carbon (TOC) content, organic carbon stable isotope ($\delta^{13}C_{org}$) of the bulk sediment and benthic foraminiferal assemblage composition and their ecological characteristics are studied to investigate the effects of Nile River discharge variability on primary productivity in the eastern Levantine Basin. Pollen data (i.e., arboreal pollen (AP) and *Artemisia*/Chenopodiaceae (A/C) ratio) are used for documenting the response of the local vegetation to Mediterranean paleoclimate and paleohydrology changes.

2. Study area

Core V-4 was extracted in 1998 within an exploration program for sand resources off the coast of Israel aimed to examine the feasibility of an Israeli-Dutch project of creating artificial islands for clusters of infrastructure (Almagor et al., 1998). The core was drilled in the southeastern Levantine shelf, 6.2 km to the west of the Alexander River off the Mediterranean coast of Israel, midway between Haifa and Tel Aviv (Fig. 1). The inner shelf sediments up to Haifa Bay are predominantly Nile-derived siliciclastics (e.g., Zviely et al., 2007). Sand extends from the foreshore to ~35 m water depth, the approximate position of the fair-weather wave base (Hyams-Kaphzan et al., 2008), and is transported primarily

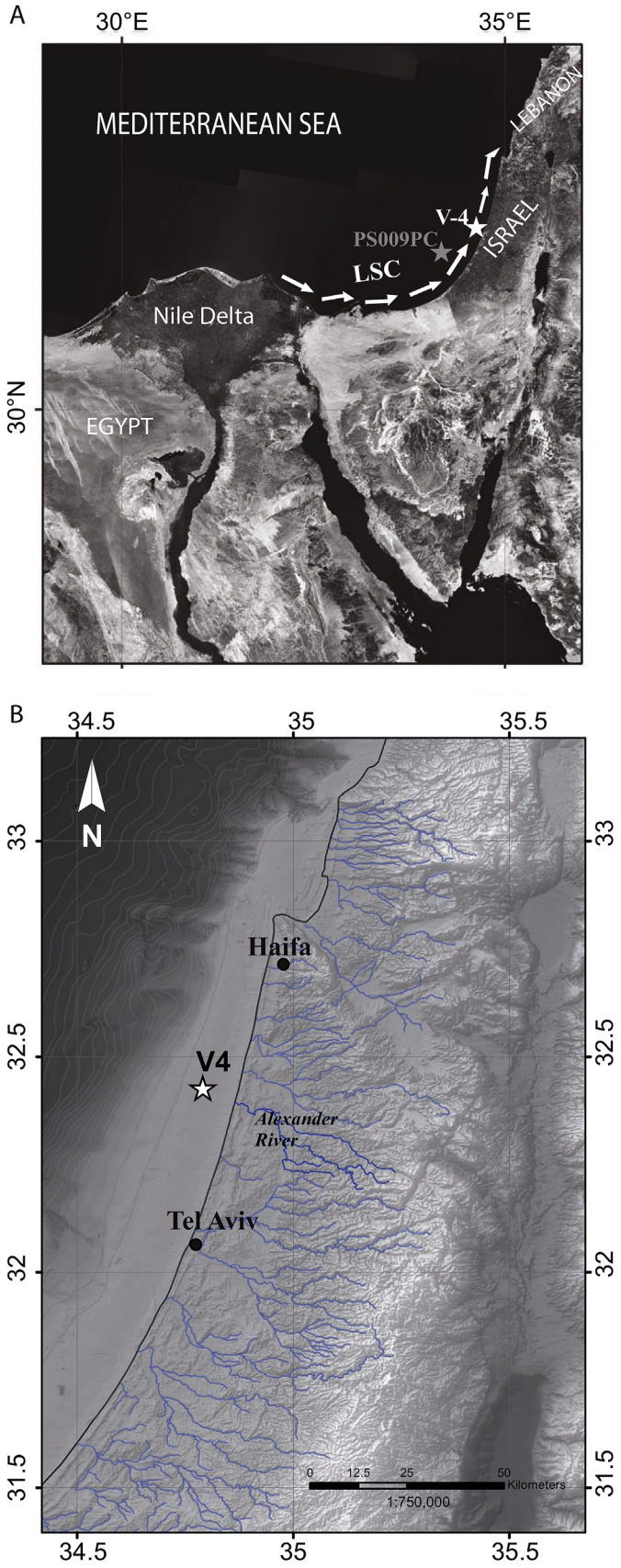

Fig. 1. (A) The study area is part of the Nile littoral cell, located at the SE Levantine Basin, which extends from the Nile Delta, Egypt to Haifa Bay, Israel. The studied core V-4 is located at the middle shelf at 46.8 m water depth, 34.809042/32.434228 close to core PS009PC (32°07.7′N, 34°24.4′E; 552 m water depth) that was studied by Hennekam et al. (2014, 2015) and used as a reference in this study. Also shown by arrows is the northeast direction of sediment transport by the prevailing longshore current (LSC). (B) The south eastern Mediterranean showing rivers and streams that flow into the coastal plain of Israel and cities marked in black dots.

northward by wave-induced longshore currents (e.g., Golik, 1993). At depths between 40 m and the shelf edge, at ~100–120 m, sand is progressively diluted by silt and clay (Almagor et al., 2000; Zviely et al., 2007; Almogi-Labin et al., 2012).

The main nutrient-rich freshwater and sediment load contributor to the SE Mediterranean Sea is the Nile (until its damming in 1965) (e.g., Said, 1993; Krom et al., 1999). The local coastal streams, notably from Tel Aviv northward are considered during recent times an additional source for nutrients and sediments, mostly of clays (Sandler and Herut, 2000). The regional freshwater budget varies as a result of the interaction between changes in the rate of evaporation, rainfall amount, and runoff (e.g., Thunell and Williams, 1989; Malanotte- Rizzoli et al., 1996).

The climate in the region is characterized by rainy winters and dry summers, and is associated with a well-defined precipitation pattern of winter rains, related to the cyclonic activity created or intensified within the Mediterranean basin (e.g., Ziv et al., 2006; Enzel et al., 2008).

At present the flow regime of the Nile incorporates the Blue Nile/Atbara Rivers (~70% Nile outflow) and the White Nile (the remaining ~30% of Nile outflow). The White Nile, that originates from the Equatorial African mountain ranges, is affected by a mixed Atlantic/Indian Ocean rainfall system. The Blue Nile and Atbara Rivers that originate from the Ethiopia Highlands have a mainly Atlantic-derived moisture source (Mohamed et al., 2005). Nonetheless, it's worth mentioning that the Ethiopian highlands as well as the eastern Mediterranean Sea and the Levant region are influenced by indirect relationships between both monsoon systems (the Asian and African monsoons) which have complex effects on the temperature regime, precipitation patterns and seasonality (Ziv et al., 2004), in addition to the Nile outflow.

Moreover, in contrast to the present-day flow regime, well dated multi-proxy records show substantial variability in Nile discharge on multicentennial - to millennial time scales, which correlates with Monsoon variations (e.g., Overpeck et al., 1996; Hamann et al., 2009; Hennekam et al., 2014). For example, during the early to middle Holocene, the increased Nile discharge correlates with the maximum strength of the Indian Ocean-influenced Southwest Indian summer monsoon (Hennekam et al., 2014).

An anticlockwise surface water circulation, the Long shore currents (LSC) along the Israeli Mediterranean coastline which is part of the Nile littoral cell moves the Nile outflow and its sediment content north-eastward (Pinardi and Masetti, 2000). At present, during most of the year the discharge from the Alexander River is extremely low (Sandler and Herut, 2000). It seems that also in the past, due to the anticlockwise surface water circulation, the contribution of this river to the core site was negligible.

3. Materials and methods

3.1. Core sampling

A continuous vibracore, V-4, 7.35 m long, was obtained abroad R/V ZIRFAEA during June, 1998 from the southeastern Levantine shelf (34.809042/32.434228) at water depth of 46.8 m (Fig. 1). This area has experienced high sedimentation rates throughout the Holocene, even in deeper parts (e.g., Krom et al., 1999; Schilman et al., 2001a,b; Almogi-Labin et al., 2009; Hamann et al., 2009; Box et al., 2011). Thus, our core site is ideal for studying the

continuity of Nile outflow preserved in sedimentary archives deposited during the Holocene and potentially helps reconstructing high-resolution (i.e., sub-Milankovitch) Holocene climatic variability within the River Nile catchment. The core was sampled continuously at 2 cm intervals along its top 10 cm, at 5 cm intervals in the upper 1.5 m and every 10 cm along the rest of its length. A total of 48 samples of 13–26 g dry weight (each) were collected for further analyses.

3.2. Dating

Eleven samples of pristine well-preserved molluscs, one sample of echinoderm spines and four samples of mixed foraminifera were dated by accelerated mass-spectrometer (AMS) ^{14}C- technique either at the Keck Carbon Cycle AMS Facility (Irvine, CA) or at ANSTO (Australian Nuclear Science and Technology Organization) (Table 1). The raw radiocarbon ages were converted to a calibrated calendar age using Marine13 curve (Hughen et al., 2004; Reimer et al., 2013), Calib 704 (Stuiver and Reimer, 1993), which incorporates a time-dependent global ocean reservoir correction of about 400 years. To accommodate local effects on the reservoir age, a mean marine reservoir correction for the local region ($\Delta R = 53 \pm 43$) was used. The results are presented with a statistical error of 2σ, or 95% confidence level (Table 1).

In order to improve precision and refine the chronostratigraphic sequences of ^{14}C ages, an age-depth model was constructed by using Markov chain Monte Carlo Bayesian methods with the program WinBacon 2.2 (Blaauw and Christen, 2011). This method incorporates a prior assumption into the model, in this case a simple stratigraphic assumption that age should increase with depth. All dates calculated by the model and presented also in Table 1 are calibrated by Bacon with the Marine13 dataset and the same local ΔR was applied to all samples.

Bacon repeatedly samples from the full probability density function of each calibrated age to fit many possible splines to the age controls, and discards fitted splines that result in age reversals. A posterior probability density function for each depth in the sediment core is generated from the population of the retained splines. We ran Bacon with normal distribution with section length of the piecewise calculated spline, set to 20 cm. Section length is not a prior parameter per se, but rather affects computational speed (more segments allow more flexibility of the model to adapt to within-core changes in sedimentation rate, but increases calculation time). At 25 cm a hiatus is provided within the Bacon command. Ages between the lowest accepted ^{14}C sample at 700 cm and the base of the core at 730 cm were calculated by linear extrapolation of the sedimentation rate of the lowest model section. The model parameters and maximum a posteriori age–depth model with 95% confidence intervals (i.e., best fit) can be found in Supplementary data No. 1 and Table 1.

3.3. Sedimentological analysis

Grain size analysis was performed with Malvern MS-2000 laser diffraction over the particle-size range of 0.02–2000 μm. We measured two sets of samples: bulk samples (without any pretreatment) and samples that were treated with H_2O_2 and 1M HCl solution to dissolve organic matter and carbonates, respectively. Measurement procedure included dispersion (using sodium hexametaphosphate solution), stirring for 5 min, and ultra-sonication for 30 s. Three to six replicate samples of each sample were then subjected to three consecutive 5 s runs at a pump speed of 1800 RPM. The laser diffraction raw values were transformed into particle size distribution using the Mie scattering model, with optical parameters of RI = 1.52 and A = 0.1. We calculated the clay/silt/sand fractions using thresholds of 6 μm and 63 μm, respectively. We chose 6 μm as the upper clay fraction threshold since several studies demonstrate that it is equivalent to the mostly used 2 μm threshold when using the sedimentation technique (e.g., Miller and Schaetzl, 2012; Fisher et al., 2017).

3.4. Geochemical analysis

For isotopic measurements of organic carbon, the carbonate fraction was removed by fumigating the samples with 12N HCl in a desiccator (at least 8 h) in silver capsules, drying them over night (at ~55 °C), and then wrapping with tin capsules. The advantage of this procedure is that it avoids direct contact between the sample and the acid, all samples get exactly the same treatment, and the carbonate fraction is (usually) entirely dissolved.

Table 1
AMS ^{14}C dating results obtained from the Keck Carbon Cycle AMS Facility (Irvine, CA) and from ANSTO (Australian Nuclear Science and Technology Organization) (Lab number begins with the capital letters OZR). Calibrated ages in calibrated (solar) years calculated using Calib 704 (Stuiver and Reimer, 1993) with the Marine13 curve (Hughen et al., 2004; Reimer et al., 2013) and a local reservoir correction, ΔR of 53 ± 43. Calibrated ages show time intervals of >95% probability distribution at 2 sigma ranges using the Calib software and the Bacon software for Bayesian age modeling in R (Blaauw and Christen, 2011) (The full Bacon age output as shown in Fig. 2 is found in Supplementary data No. 1).

Lab no.	Depth (cm)	Dated Material	δ^{13}C PDB [‰]	^{14}C activity [pMC]	^{14}C Age [yr BP]	Cal. yr BP range, 95.4% [2σ]	Cal. Age [Median]	Error	Bayesian model ages yr BP [2σ]
OZR513	8	*Abra longicallis*	0.9 ± 0.1	98.88 ± 0.31	90 ± 25	Recent			0.035
168417	25	*Corbula gibba*			2755 ± 15	2297–2574	2436	138.5	2.581
168418	40	*Plagiocardium* sp.			2775 ± 20	2311–2639	2475	164	2.622
168419	45	Foraminifera			2960 ± 20	2508–2774	2641	133	2.635
168420	95	*Corbula gibba*			3000 ± 20	2638–2838	2738	100	2.783
168421	115	Foraminifera			3880 ± 15	3637–3904	3771	133.5	2.871
168422	125	Foraminifera			3810 ± 15	3567–3822	3695	127.5	2.921
OZR514	135	*Nuculana pella*	1.2 ± 0.1	66.58 ± 0.23	3270 ± 30	2866–3175	3021	155	2.961
OZR515	200	*Corbula gibba*	1.1 ± 0.2	66.04 ± 0.22	3335 ± 30	2945–3270	3108	163	3.154
OZR516	230	*Corbula gibba*	1.5 ± 0.1	65.5 ± 0.23	3400 ± 30	3050–3347	3199	149	3.240
OZR517	300	*Nucula* sp.	2.2 ± 0.2	64.31 ± 0.21	3545 ± 30	3228–3510	3369	141	3.460
OZR518	320	*Echinoderm spine*	1 ± 0.3	62.57 ± 0.21	3765 ± 30	3489–3799	3644	155	3.542
OZR519	460	*Corbula gibba*	0.8 ± 0.1	61.15 ± 0.22	3950 ± 30	3707–4038	3873	166	3.900
OZR520	660	*Nuculana pella*	0.1 ± 0.1	58.54 ± 0.23	4300 ± 35	4180–4507	4344	164	4.385
OZR521	700	*Corbula gibba*	1.8 ± 0.1	58.44 ± 0.18	4315 ± 30	4213–4518	4366	153	4.482
168423	733	*Foraminifera*			3955 ± 15	3720–4020	3870	150	4.555

Nitrogen isotopes were measured on 40–80 mg aliquots of homogenized powdered sample with a mean standard deviation based on replicate analysis of samples of 0.5‰ for $\delta^{15}N$. The organic $\delta^{13}C$ mean standard deviation based on replicate analysis of samples is of 0.3‰.

The organic C and N samples were measured on Flash 2000 Organic Elemental analyzer in line with Thermo Finnigan Delta V plus stable isotope ratio mass spectrometer (IRMS). All results were reported relative to VPDB for $\delta^{13}C$ and relative to air for $\delta^{15}N$.

C/N ratios of organic matter have been widely used as a reliable parameter to distinguish between marine algal source and land-plant origins of sedimentary organic matter (e.g., Hedges et al., 1986; Twichell et al., 2002). Ratios for terrestrial plant biomass range widely, from values of ~20 (grasses) to ~200 (trees) (Hedges et al., 1986). Within soils, C/N values vary among pools dominated by different classes, and relatively high values (e.g., >100) tend to be preserved in resilient particulates (e.g., black carbon; Schmidt and Noack, 2000), whereas mineral-bound compounds tend to exhibit lower values (~5–20) (Sollins et al., 2006). Marine organic matter commonly has C/N values lower than 10 (Hedges et al., 1986).

3.5. Foraminiferal analysis

Samples were washed through 63 μm sieve, and dried at 50 °C. From each sample at least 200–300 benthic foraminiferal specimens (>63 μm) were picked from a split aliquot representing the entire sample (Supplementary data No. 2). Specimens were identified to species level and counted to determine the species relative abundance, species richness, species diversity (i.e., Fisher α-index) and dominance (Fisher et al., 1943; Levin and Gage, 1998). The state of preservation of the tests was evaluated and is usually very good throughout the studied sequence. Taxonomic identification was based mainly on Cimerman and Langer (1991) and Sgarrella and Moncharmont-Zei (1993).

3.5.1. Statistical analysis

Q-mode cluster analysis (CA) was processed by PRIMER version 6 software (Plymouth Routines in Multivariate Ecological Research, UK). The data of the relative abundance of the common benthic species (>3%), Square root transformed in order to down-weight the relative contribution of dominant and abundant species. These transformed abundances were used to build a similarity matrix based on Bray–Curtis similarity, and to reconstruct a dendogram showing hierarchical clustering (group-average linkage) and a non-metric multi-dimensional scaling (MDS) ordination. In order to further test the correlation between the species distributions we used the parametric correlation coefficient Pearson's *r* overlain the MDS biplot. 'Similarity profile' (SIMPROF) permutation tests were used to identify significant groupings, so that the all-retained groups had a significant ($P < 0.05$) internal structure. A 'similarity percentages' (SIMPER) routine was used in order to identify species that contributed most to the similarity within each cluster, as well as to dissimilarities with other clusters.

3.6. Palynological and charcoal analyses

Standard methods (Faegri and Iversen, 1992) have been used for the preparation of samples for pollen analysis and for pollen counting. Pre-treated *Lycopodium* spore tablets were added to each subsample to calculate pollen accumulation rate values (Stockmarr, 1971). Pollen identification was based upon the UCLA pollen reference collection and published references (Moore et al., 1991; Reille, 1995, 1998, 1999; Beug, 2004). Total pollen sum of terrestrial plants is the basal sum for calculating percentages, total pollen concentrations (grains/cm^3) and total pollen accumulation rates (grains/cm^2/year). This is the default pollen sum used in the Tilia program (Grimm, 1990). The arboreal pollen (AP) and the non-arboreal pollen (NAP), pollen frequencies (%) as well as individual pollen taxa frequencies (%) and their accumulation rates were determined. Pollen from Pinaceae, particularly *Pinus*, is often greatly overrepresented especially in marine sediments, owing to higher production, greater resistance to degradation and capacity for long-distance transportation compared to other taxa (Rossignol-Strick and Planchais, 1989; Cheddadi and Rossignol-Strick, 1995b). Although our core V-4 is located in the mid-shelf the arboreal pollen (AP) frequencies and accumulation rates were calculated both including and excluding *Pinus*. The *Artemisia*/Chenopodiaceae (A/C) ratio was determined and can arguably be used as an indicator of effective moisture in arid and semi-arid regions where these plants are dominant (e.g., Liu et al., 1999), based upon the premise that *Artemisia* can require more water than members of the Chenopodiaceae during the growing season.

Subsamples (1 cm^3) were taken for macroscopic charcoal analysis at consecutive 1 cm intervals using a volumetric sampler. Charcoal samples were processed with a modified version of the protocols described by Whitlock and Larson (2001). First, samples were treated with 6% H_2O_2 at 50 °C for 24 h. Ethanol was added to clay-rich samples to prevent clay and charcoal particles from sorbing up the sides of the flasks and adhering during heating. Samples were screened through nested 125 μm and 250 μm sieves; the >250 μm portion of each sample was counted wet on the sieve and then discarded, and the 125-to-250 μm portion was rinsed with 6% H_2O_2 into plastic Petri dishes. ~2 mL detergent solution (dilute [0.5%] sodium hexametaphosphate) was added to each dish to disperse charcoal which then placed in the drying oven at 50 °C until all liquid was evaporated and charcoal particles adhered to the dish surface. Petri dishes were placed on a gridded platform for counting. Charcoal counts were converted to charcoal influx or charcoal accumulation rates (CHAR) by multiplying concentrations (particles per cubic centimeter) by the estimated sedimentation rate for each sample.

Charcoal analysis of marine sediments (among other depositional environments) is used to reconstruct long-term variations in fire activity which is controlled naturally by climate variability and vegetation characteristics or by anthropogenic influence (e.g., Power et al., 2010 and references therein). Stratigraphic levels with abundant charcoal (so-called charcoal peaks) are inferred to be evidence of past fires. In this study charcoal data are used to complement and extend reconstructions provided by integrating the chronological and the above multi-proxy records.

4. Results

4.1. Dating

The Bayesian age model was constructed based on all twelve AMS dates of well-preserved single taxa, mostly molluscs, with good agreement between ages while stratigraphic order is maintained (Fig. 2, Table 1). The four hand-picked mixed benthic foraminiferal ^{14}C samples (at 733, 125, 115 and 45 cm) with age reversals were excluded from the model (Table 1). It is worth mentioning that we did not have enough material to undertake ^{14}C measurements on single taxa as recommended by Magana et al. (2010). This latter study shows that some mixed benthic foraminiferal samples may result in offsets ages due to the occurrence of

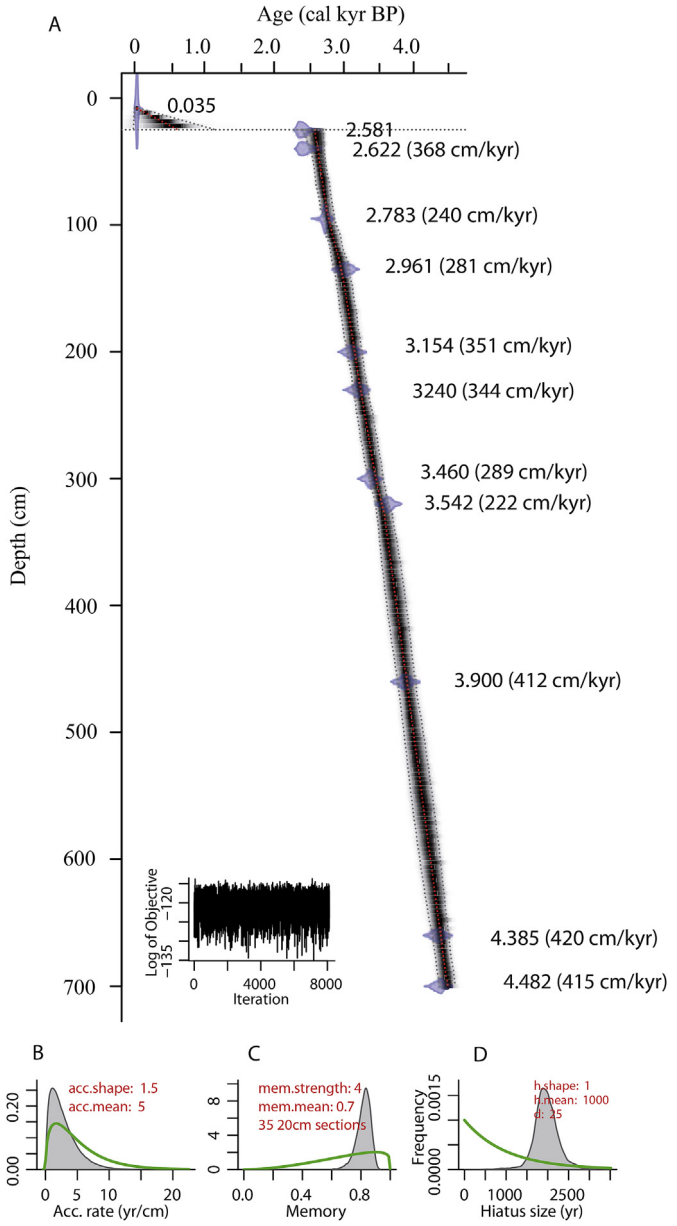

Fig. 2. Age model. Bayesian age model output from Bacon (Blaauw and Christen, 2011), based on the probability density function for each calibrated radiocarbon age (A). The calibrated ^{14}C dates (transparent blue) and the age-depth model (darker greys indicate more likely calendar ages; grey dotted lines show 95% confidence intervals [error ranges]; red dotted curve shows single "best" model based on the weighted mean age for each depth). Supplement figures show the prior (green curves) and posterior densities (grey histograms) for the mean accumulation rate (B; sedimentation rate) the memory (C; autocorrelation strength at 1 cm intervals), and the time gap (D; hiatus size), the prior estimates in the age model. Estimates of accumulation rates produced by the age-depth model are given in parentheses near each calibrated ^{14}C dates (the full Bacon age output is found in Supplementary data No. 1). (For interpretation of the references to color in this figure legend, the reader is referred to the Web version of this article.)

infaunal taxa which may be biased anomalously due to calcification process in old pore waters. We hypothesize that similar process may have produced these offsets in ^{14}C ages, making our radiocarbon dates of mixed foraminifera questionable.

Nevertheless, our age-depth model provides a high-resolution calibration curve constraining the age of most of the sedimentary sequence of core V-4 as Mid - to Late Holocene from 4.5 to 2.6 cal kyr BP (Supplementary data No. 1, Table 1, Fig. 2). The upper 25 cm represent deposition during the last ~2.6 kyr BP considering a possible hiatus and/or lack of preservation.

4.2. Sedimentological and geochemical properties

The sedimentary sequence (penetrated in the V-4 borehole) is subdivided into three main units and transitional phases between them based on the sedimentological and geochemical characteristics and the estimates of sedimentation rates produced by the age-depth model. The lower unit (~3.5 m thick, between 7.35 and 3.9 m), Unit I, is composed of clayey-silty sediments (51–61% silt). It was deposited from 4.5 to ~3.7 cal kyr BP, at almost constant and high sedimentation rates (422–400 cm kyr^{-1}) (Fig. 3). This unit is characterized by moderate fluctuations in TOC content (0.6–1.1 wt.%), and in relatively low carbonate content (13–23 wt.%) and by stable total organic nitrogen (TON) and C/N ratio values (0.05–0.07 wt.% and 11.4–18.3, respectively) (Fig. 3). The lowest TOC value (0.6 wt.%) in this unit, together with almost complete disappearance of the carbonate-free sand is followed by a sharp increase in $\delta^{15}N_{org}$ value from 5.1‰ to 9.4‰ at 4.28 kyr BP. The transition phase to the middle unit, (Unit II) at ~ 3.6 kyr BP, is characterized by a sharp decrease in sedimentation rates (246 cm kyr^{-1}) along with an increase in the clay fraction, a drop in the TOC value (0.6 wt.%) and a decline in C/N ratio to a value below 10 and simultaneous increase rise of $\delta^{15}N_{org}$ from 5.7‰ to above 9.1‰ (Fig. 3).

Unit II (~2.2 m thick, between 3.5 and 1.3 m), deposited between from ~3.6 to 2.9 cal kyr BP, shows recurrent noticeable fluctuations especially in the TOC and carbonate contents, and in the C/N ratio and the organic C isotopic record. Prominent TOC maxima (usually >1 wt.%, apart from one event) associated with higher carbonate and C/N values (>20 wt.% and between 19 and 22 respectively), lower $\delta^{13}C_{org}$ values (between −19 and −20‰) and a decrease in sedimentation rates (in two events) occurred at 3.5, 3.3, 3.2 and 3.0 kyr BP (Fig. 3). At the transition to the upper unit, Unit III, at 2.9 cal kyr BP, the $\delta^{15}N_{org}$ values rise to 7.3–8.3‰, similar to earlier higher records observed at ~3.6 and 4.2 cal kyr BP.

Unit III (~0.9 m thick, between 1.15 and 0.25 m) was deposited between 2.8 and 2.58 kyr BP. The base of this unit exhibit increase in sedimentation rates that reach a high and steady value of ~365 cm kyr^{-1}. Above this unit, the upper part of the core includes the highest sand content reaching 19% and a decreasing TOC content from 0.81 to 0.46 wt.%.

4.3. Foraminiferal characteristics

The sedimentary units distinguished by the unique sedimentological and geochemical features have also prominent foraminiferal characteristics (Fig. 4). The Q-mode cluster analysis, based on the 48 samples (with foraminiferal counts between 235 and 735 specimens per sample) and 21 foraminiferal taxa (with >3% relative abundance, out of the 70 species identified), displayed three distinct clusters (Fig. 5A, Supplementary data No. 2) and one outlier (the upper sample). The distribution of the three sample clusters along the core generally mimics the subdivision of the sedimentary sequence into 3 main units apart from two samples close to the transition from Unit I to Unit II (at 3.80 and 3.90 cal kyr BP which are part of cluster II instead of cluster I) (Figs. 4 and 5A). The fields of the three main sample clusters on a multi-dimensional scaling (MDS) diagram are separated with one sample overlaps between clusters 1 and 2 (Fig. 5B). The outlier identified in the dendrogram (Fig. 5a) is also shown in Fig. 5B. The SIMPER routine highlighted three major sample clusters with more similarities between cluster 1 and 3 (Supplementary data No. 3). The most significant species contributing to each cluster are listed in order of descending average relative abundance in Fig. 5A.

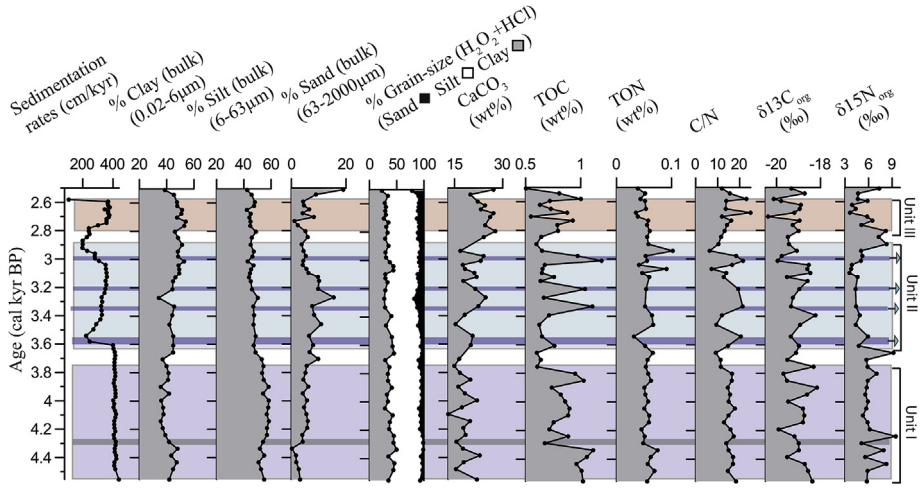

Fig. 3. Sedimentological and geochemical characteristics of Core V-4 vs. age including sedimentation rates produced by the Bacon software for Bayesian age modeling, clay silt, and sand content (wt.%) (grain size is also shown after carbonate and organics removal), $CaCO_3$ (wt.%), TOC (wt.%), TON (wt.%), C/N, $\delta^{13}C_{org}$ (‰) and $\delta^{15}N_{org}$ (‰). The main climatic phases are indicated; in pale blue - (Unit I) an arid and stable Mid-Late Holocene climate between 4.5 and 3.58 cal kyr BP with a maximum peak in aridity at 4.28 kyr BP in dark grey; in light blue (Unit II) - an unstable late Holocene climate between 3.58 and 2.8 cal kyr BP with wetter conditions and increased runoff especially of the Nile River at 3.58, 3.3, 3.2 and 3.0 kyr BP in dark blue and arrows pointing up; in light pink a return to a relatively arid phase between 2.8–2.6 cal kyr BP. (For interpretation of the references to color in this figure legend, the reader is referred to the Web version of this article.)

Foraminiferal abundance was relatively stable and low in the clayey-silty sediments of Unit I (cluster sample I), between 4.5 and ~3.7 cal kyr BP, where it never exceeded 42 individuals per gram dry sediment (ind./g). Additionally, samples in this unit had moderate stable dominance values of 18–30%. Cluster I which encompasses the samples of Unit I, is characterized by the dominance of *Porosononion subgranosus* (21% of the assemblage on average) and *Cribroelphidium poeyanum* (18% of the assemblage on average) accompanied by other species such as *Nonionella turgidus* (10% of the assemblage on average) (Fig. 5A). Moreover, *Ammonia inflata* show a distinct decrease towards the top of Unit I. Some species such as *N. turgidus* occur in their highest concentrations in the sediments deposited before 4.28 kyr BP, when a marked decrease in TOC values from generally high and stable values is observed. At the same time, however, species such as *C. poeyanum* and *Valvulineria bradyana* declined in their abundance (Fig. 4B).

In Unit II, between ~3.6 and 2.9 cal kyr BP, foraminiferal abundance and dominance displayed large scale and frequent changes varying between 26 and 113 ind./g, and 21 and 63%, respectively, with highest values coinciding with high TOC values, at 3.3, 3.2, and 3.0 cal kyr BP (Figs. 3 and 4). The foraminiferal cluster II occurring during this unit is dominated by *Ammonia tepida* (40% of the assemblage on average) and accompanied by other species such as *P. subgranosus*, and *C. poeyanum*, though in lower numbers than in the underlain sedimentary Unit I (Figs. 4B, 5A and 5B).

The samples at the transition interval between Units II and III, at 2.9 cal kyr BP, and the samples of Unit III and the overlying recent sediments, all were clustered together (in cluster III) (Fig. 5). Nonetheless, there are some differences in the foraminiferal abundances and species composition. Samples deposited between 2.9 and 2.6 cal kyr BP are characterized by a return to a relatively low foraminiferal abundance and dominance values similar to the values of Unit I, at the base of the core; however, with a noticeable occurrence of some species such as *C. poeyanum* and *Bulimina aculeata*, particularly at the transition to Unit 1 (Fig. 4B). The highest foraminiferal abundance and species richness were found in the transition to the recent sediments reaching maximum values of 168 ind./g and 39 species per sample, respectively, parallel to the decrease in sedimentation rates (Figs. 3 and 4, Supplementary data No. 2). The foraminiferal assemblage included species that occur at their highest numbers along the sequence such as *Ammonia beccarii*, *Asterigerinata mamilla*, and *Triloculina marioni* (Fig. 4B).

4.4. Pollen and charcoal data

The three sedimentary units distinguished by all of the above mentioned proxies (Figs. 2–5) show some variations predominantly in pollen concentrations, accumulation rates, AP values and A/C ratio. However, the stratigraphies have a high degree of variability throughout the section. Pollen concentrations and accumulation rates in Unit I are the highest along the sequence with values fluctuating between 2198 and 8138 grains/cm^3 and between 906 and 3331 grains/cm^2/year, respectively (Fig. 6, Supplementary data No. 4). AP values and A/C ratios fluctuated in this unit with a notable decrease to zero in both parameters at 4.28 kyr BP (Fig. 6 A and B).

Pollen concentrations and accumulation rates are similar in Units II and III and relatively lower compared to their values in Unit I. Nonetheless, pronounced sharp and drastic fluctuations in A/C ratios characterize Unit II sediments (i.e., compared to the relatively more stable values in Unit III) with peaks corresponding to higher pollen concentrations and accumulation rates at 3.5, 3.2 and 3.0 kyr BP (Fig. 6 A and B).

Charcoal influx or accumulation rates were variable along the entire core. However, the most noticeable fluctuations especially were observed in Unit II (~200–7000 particles cm^2/y) where a single peak in CHAR with a magnitude several times higher (~30,500 particles cm^2/y) than the other peaks is also observed (Fig. 6 B).

5. Discussion

5.1. Climate variability impacts on paleoceanographic characteristics as inferred from the multi-proxy records

Marine sediment cores from tectonically stable areas with nearly flat sea bottoms such as the shelf area (Almagor et al., 2000) where core V-4 is located (Fig. 1) typically provide a continuous sedimentary sequence. The sedimentation rates in such cores are subjected to lateral and temporal variations in the hydrography and

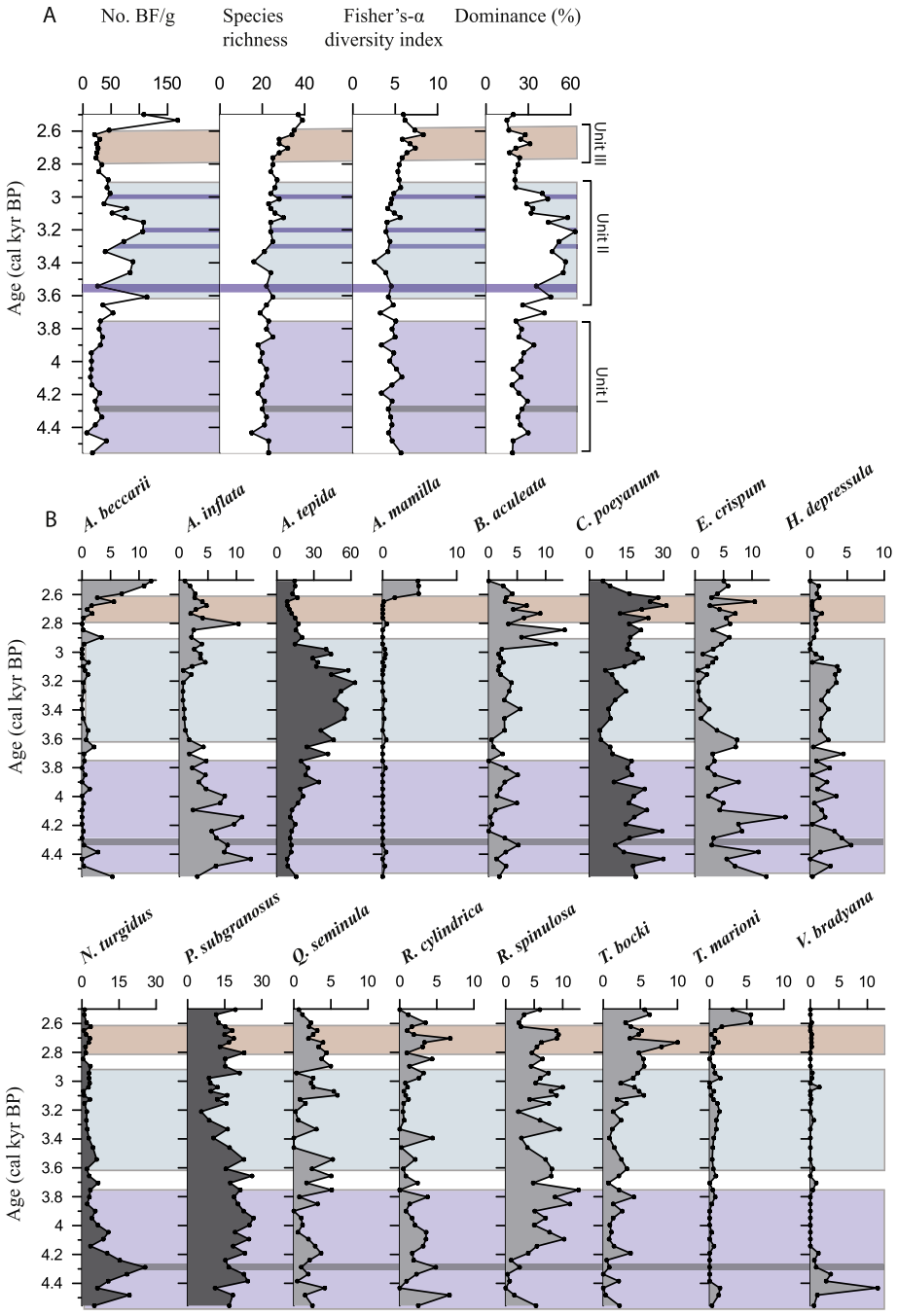

Fig. 4. Foraminiferal characteristics of Core V-4 vs. age (A) and the relative abundance of the common foraminiferal species (>5%) (B). Subdivision into Units used in the text are denoted end explained in the caption of Fig. 3.

sedimentation patterns due to global and regional climate fluctuations. Exceptionally high sedimentation rates ranging between 246 and 422 cm kyr^{-1} were calculated for different parts of core V-4 (Fig. 2), providing an unprecedented high resolution sedimentary archive. Since most of the samples in this core were sampled at intervals of 10 cm, equivalent to a resolution of 24–40 years, multi decadal to centennial-scale variability in sediment supply, hydrological regime, climate change, and vegetation cover can be established. Additionally, our data could be compared with the southeast Levantine Basin core PS009PC studied by Hennekam et al. (2014) which has a similar high resolution record of ≤40 years.

Closer to the coast, at somewhat shallower water depths (~35 m), both at the southern and the central parts of the Israeli coast higher sedimentation rates (~140 cm kyr^{-1}) occur during the early Holocene decreasing to lower rates (<60 cm kyr^{-1}) during the late Holocene (Tapiero, 2002). Consequently, the sedimentary archive preserved in core V-4 is the only record known from the southeastern Mediterranean shelf with such high sedimentation rates.

Sea level in the south-eastern Mediterranean Sea stabilized at ~6–4 ka (Sivan et al., 2001) reaching its present level at ~3.6 ka (Porat et al., 2008). Based on the comparison of our age model with the Holocene sea-level curve of the Mediterranean coast of Israel (Sivan et al., 2001) and taking into account the length of the core it

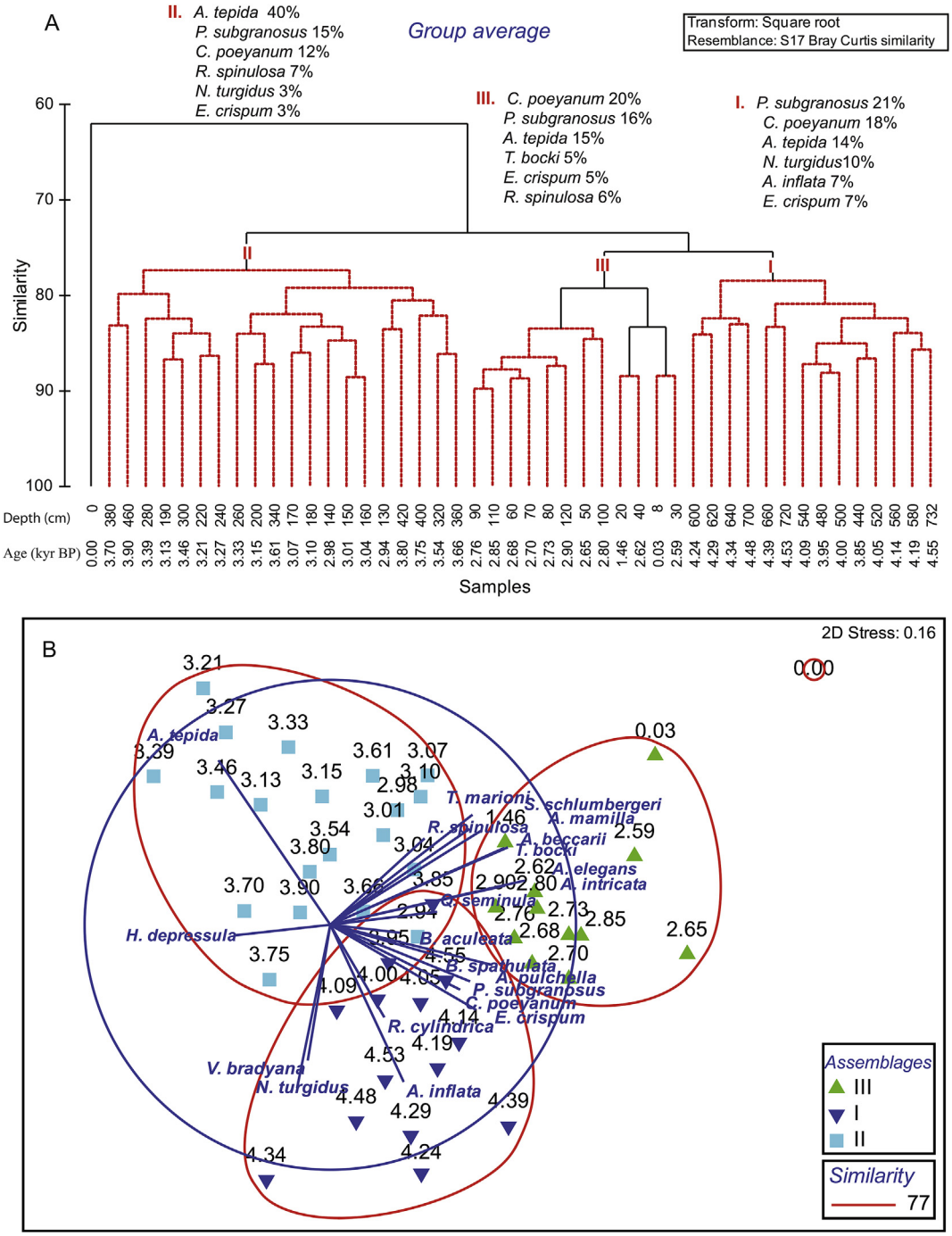

Fig. 5. Dendrogram of Q-mode cluster analysis (CA) of the 47 samples from core V-4 using group-average linking of Bray–Curtis similarities calculated on square root transform benthic foraminiferal abundance >3%. Taxa that make significant contributions (in descending order) to the similarity within each cluster, based on SIMPER routine (Supplementary data No. 3), are shown, with their raw average abundances (A). Non-metric multi-dimensional scaling (MDS) illustration in two dimensions computed using the same similarity matrix of the hierarchical clustering (Fig. 5A) overlain by a parametric correlation coefficient Pearson's *r* measuring the correlation between the species distributions (B). Both CA and MDS illustrations show relatively good separation of the three assemblages and one outlier.

seems that the base of the sedimentary sequence in core V-4 accumulated at a water depth deeper only by 1–2 m compared with the current water depth.

We utilized multi-proxy marine derived records including sedimentological, geochemical, foraminiferal and organic stable isotope data to reconstruct Mid - to Late Holocene northeast African climate variability. Combining these proxies enables us to identify stable arid phases as well as periods of unstable conditions characterized by fluctuations between wetter and drier conditions. These climate variations are driven by the monsoonal system leading to changes in Nile outflows which impact the ecological conditions within the Nile littoral cell. The land-derived records, i.e., the pollen is an important proxy for climate change which adds some information on a local scale on changes in the Mediterranean

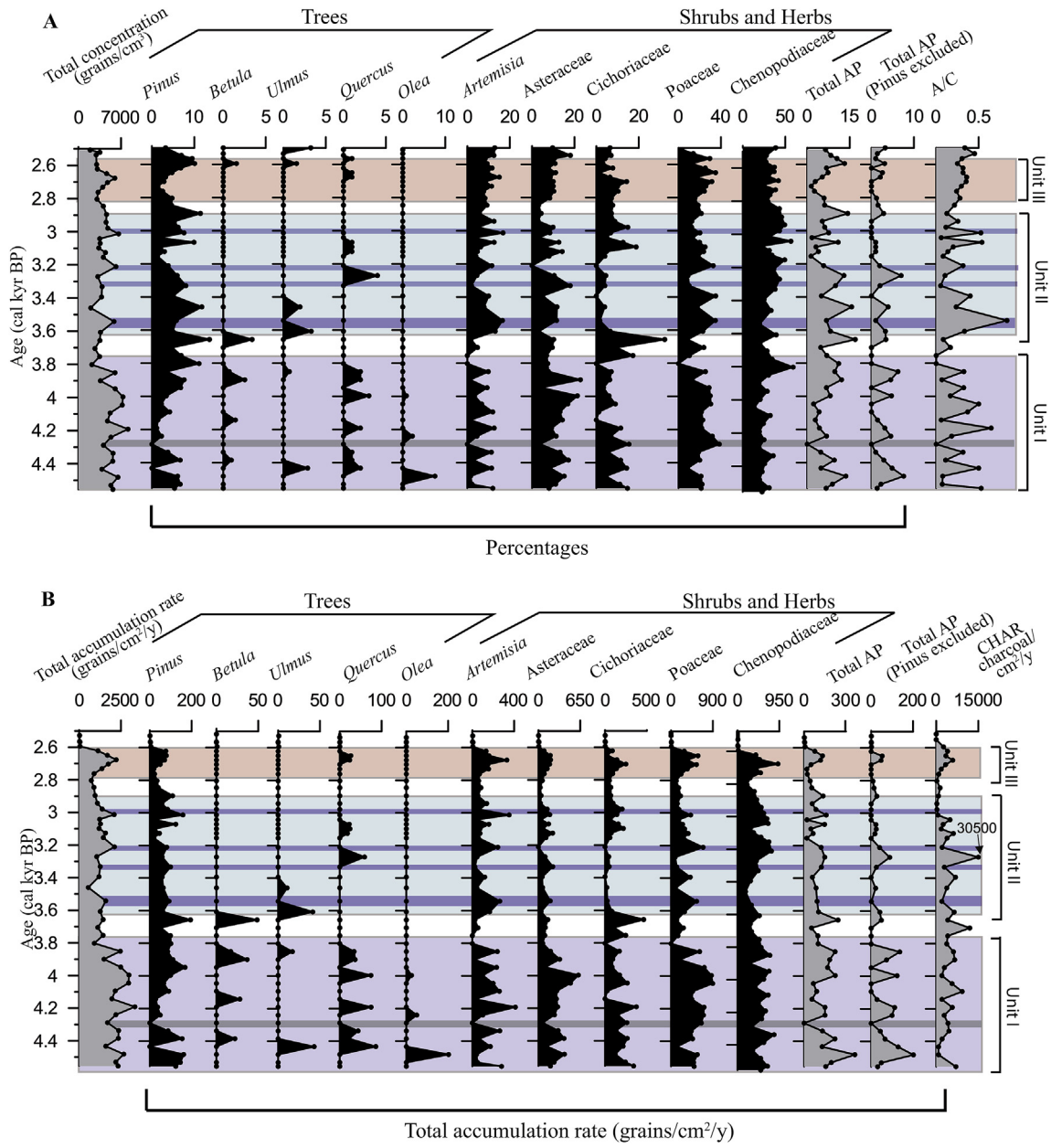

Fig. 6. The pollen record of Core V-4 vs. age. Total pollen sum of terrestrial plants is the basal sum for calculating percentages, concentrations (grains/cm^3) (A) and accumulation rates (grains/cm^2/year) (B), based on the age–depth model (the default pollen sum in the Tilia program) (Grimm, 1990). The arboreal pollen (AP) and the non-arboreal pollen (NAP) as well as pollen types frequencies (% type out of AP +NAP) and their accumulation rates were determined (A). Pinaceae, particularly *Pinus*, are greatly overrepresented especially in marine sediments, owing to their higher resistance to degradation during long-distance transportation (e.g. Rossignol-Strick and Planchais, 1989; Cheddadi and Rossignol-Strick, 1995b). Although our core is located in the middle shelf the arboreal pollen were also recalculated while excluding *Pinus*. The *Artemisia*/Chenopodiaceae (A/C) ratio is given in A and charcoal accumulation rates (CHAR) in B.

climate system. Nonetheless, climatic inferences from pollen data for periods that are known to be human impacted, need to be considered with cautious.

The periods from 4.5 to ~3.6 and 2.8 to 2.58 cal kyr BP (Units I and III in core V-4, respectively) are characterized by high and constant sedimentation rates and relatively constant values with occasional weak to moderate fluctuations (compare to Unit 2 sediments, deposited between ~3.6–2.8 cal kyrBP) in all the proxies investigated in this study (Figs. 3–6). We interpreted these intervals as fairly stable phases within a known arid Mid-to-Late Holocene period compared to the wet Early Holocene associated with the enhanced monsoon system (Hennekam et al., 2015 and references therein) and also with the Mediterranean climate system (e.g., Bar-Matthews et al., 2003; Enzel et al., 2003; Langgut et al., 2011) (Figs. 3 and 7). Our interpretation is based on evidence of climate changes in the Nile catchment which is considered the major source of nutrient-rich freshwater and sediment load draining into the eastern Mediterranean Sea (until the Nile damming in 1965) (e.g., Adamson et al., 1980; Said, 1993; Krom et al., 1999, 2002). Based on the analysis of major element geochemistry, these latter studies have shown that there is an inverse relationship between Nile River flow and Blue Nile/Atbara sediment input. Drier climate periods during the past ~4000 years are typified by a reduction of vegetation cover and, therefore,

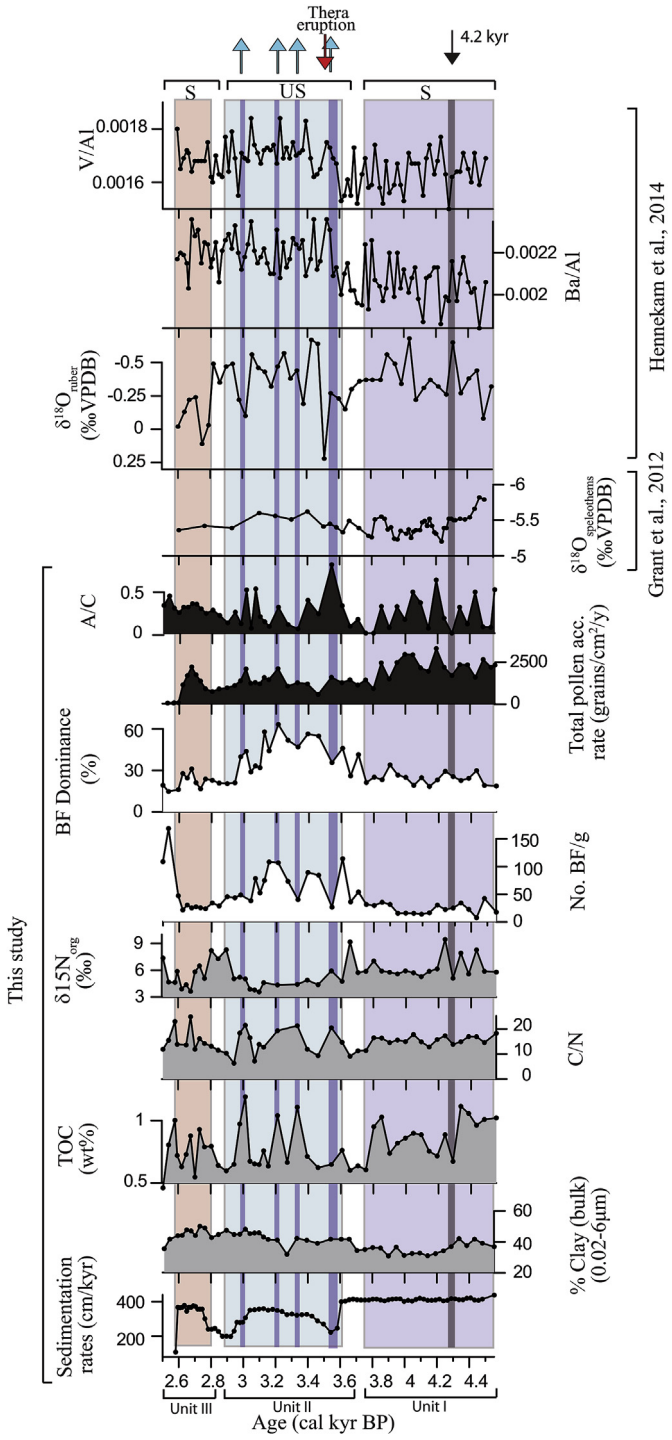

Fig. 7. Mid-Late Holocene climatic events based on 9 proxies analyzed in the current study compared with the $\delta^{18}O$ record of Soreq cave deposits (Grant et al., 2012) and with the $\delta^{18}O_{G.\ ruber}$, Ba/Al, and V/Al records of core PS009PC (Hennekam et al., 2014). Subdivision into Units used in the text are denoted end explained in the caption of Fig. 3. The distinct transition from a stable (S) to an unstable (US) climate regime at 3.58 kyr BP may have been triggered by the Thera eruption denoted in red arrow pointing down. (For interpretation of the references to color in this figure legend, the reader is referred to the Web version of this article.)

enhanced erosional processes in the Ethiopian Highlands and lowlands resulting in an increase in sediment influx, while marked by a decrease in sediment influx during wet periods and higher river flow (Krom et al., 2002; Hennekam et al., 2014). These changes, documented in slope sedimentary archives, were probably caused by a shift of the Inter Tropical Convergence Zone, southward or northward, resulting in a decrease or increase in vegetative cover over the Ethiopian Highlands due to reduced or enhanced rainfall, respectively. Stalagmite-based oxygen isotope profiles from Oman and Yemen suggest that during the middle to late Holocene the summer ITCZ continuously migrated southward and monsoon precipitation decreased gradually in response to decreasing solar insolation (Fleitmann et al., 2007). Other monsoon records from the Indian and East Asian monsoon domains show similar trend nevertheless with occasional abrupt short duration events superimposed on this general long-term gradual trend (Fleitmann et al., 2007 and references therein).

The precession-forced insolation changes influencing the low latitude monsoonal activity (Rossignol-Strick et al., 1982; Rossignol-Strick, 1985; Rohling, 1994). Thus, our record adds new information on the last African monsoon precession subperiodicity.

The environmental stability interpreted for the deposition of these sedimentary intervals (4.5–~3.6 and 2.8 to 2.58 cal kyr BP) is also supported by C/N values. Variability in C/N ratios reflect varying sources of organic matter, with C/N ratios of 20 + indicating macrophytic, vascular plants origin (typified by significant proportion of cellulose rich/protein poor plant matter) whereas ratios in the range 4–10 represent algae (Meyers and Teranes, 2001). C/N values during the deposition of units III and I (apart from two excursions of high values) are between 11–18 and 11–15, respectively. These values (especially between 2.8 and 2.58 cal kyr BP) suggest the dominance of marine algal material supplemented with minor contribution of land-based material.

Unit II in core V-4 deposited between ~3.6 and 2.9 cal kyr BP is characterized by marked fluctuations in most properties measured (including: C/N ratios, TOC values, grain-size distribution, foraminiferal data, pollen concentrations and A/C ratios), thus, we interpret this interval as a period of environmental instability (Figs. 3–6 and 7). Noticeable shifts in C/N ratios coupled with C/N values exceeding 20 generally associated with the highest TOC values and lower sedimentation rates may indicate input of terrestrial organic matter (Kohn (2010); Figs. 3 and 6). The $\delta^{13}C_{org}$ values also fluctuated in response to a rise in C/N values showing lower values between −19.5‰ and −20.39‰. Although these values are considered as marine organic signal, it is noticeable that lower C/N values are compatible with higher $\delta^{13}C_{org}$ values around −19‰ to −18.1‰. Hence the lower $\delta^{13}C_{org}$ values (19.5‰ to −20.39‰) may indicate some mixing between dominant marine organic matter with some terrestrial organic matter with lower isotopic signals.

The maximum C/N events at 3.5, 3.3, 3.2 and 3.0 kyr BP are indicative of wetter conditions and higher Nile River discharge. Wetter conditions and increased river runoff delivers nutrients to the sea-water (e.g. Said, 1993; Krom et al., 1999; Schilman et al., 2001a,b). Consequently, the C/N maximum organic-rich events correlate with high productivity due to periodically enhanced supplies of nutrients and particulate organic matter via the Nile River (Schilman et al., 2001b); an interpretation which is reinforced by foraminiferal data (Fig. 4). The C/N maximum organic-rich events also correlate, in the case of the three distinct peaks, with low foraminiferal abundances and relatively higher dominance values (Fig. 4). Commonly, unfavorable (stressed) environmental conditions are reflected by low foraminiferal abundance and high dominance values (Buzas and Gibson, 1969; Murray, 1991; Jorissen, 1988). An example for stressed conditions occurs at times when a marine environment becomes eutrophic with an overload of organic matter leading to severe stress in O_2-concentrations culminating in decreasing foraminiferal abundance (Hyams-

Kaphzan et al., 2009). During such conditions the foraminiferal assemblage is characterized by the high yet unstable dominance of small numbers of opportunists which are adapted to lower O_2 concentrations (Hyams-Kaphzan et al., 2009). The scenario of periods characterized by floods delivering higher supply of nutrients leading to increased productivity of the water column is evident in the fluctuations in these parameters as recorded in Unit II (between ~3.6 and 2.9 cal kyr BP). The dominant species *Ammonia tepida* and *Cribroelphidium poeyanum* correspond to the maximum organic-rich events (Fig. 4, supplementary data No. 2). These are common, widespread species in the eastern Mediterranean shallow shelf, which are known for their close relationship to high TOC and low O_2 concentrations (e.g., Hyams-Kaphzan et al., 2009; Avnaim-Katav et al., 2013, 2015, 2016a, b; Tadir et al., 2017). *A. tepida* behaves as an opportunist species, peaking at the surface when food resources are abundant. Furthermore it can migrate deeper into the sediment and survive in very low O_2 conditions, nearly in anoxia, and when the bottom is better oxygenated – it is replaced by other species (Hyams-Kaphzan et al., 2009).

In Unit II during C/N minima of <10 an opposite trend, for all the above discussed parameters, is observed interpreted as a weakened monsoonal system, drier conditions and lower contribution of Nile River flow at ~3.4, 3.27, 3.1 and 2.9 kyr BP.

The land-derived records i.e., pollen records from the Eastern Mediterranean Sea serve as direct indications for the paleo-vegetation and paleoclimate of the Levant and nearby area (Cheddadi and Rossignol-Strick, 1995a; Langgut et al., 2011). Total AP, oak trees and *Artemisia* were found as good palynological markers for the identification of long term climatic changes, i.e., humid and dry cycles (e.g., Langgut et al., 2011). High pollen abundance of deciduous trees, i.e., *Quercus*, signals wet conditions in the mid-uplands (about 700 m to 1,200 m above sea level) of the source area, southern Greece and Italy whereas of the *Artemisia* indicates semi-arid conditions in the lowlands (Beug, 1975). In the current study, the pollen record representing Mediterranean climate system is somewhat in accordance with the marine proxies which are associated with the monsoon system. In general, the fluctuating pollen curve in core V-4 illustrate a general decreasing trend in total AP accumulation rates (Fig. 6 B) and abundance of *Olea* together with higher *Artemisia* values (Fig. 6 A). These trends are in agreement with pollen data presented by Langgut et al. (2011) which characterize the last 5000 years and represent a slight reduction in the available local moisture. Increase $\delta^{18}O$ cave deposits (another land derived proxy) indicative of a gradual decrease in rainfall also support regional desertification (e.g., Bar-Matthews et al., 2003; McGarry et al., 2004; Grant et al., 2012, Fig. 7). Despite this general climate trend, previous studies demonstrated that the Holocene displays climate variations and that it is less stable than previously considered (e.g., Bianchi and McCave, 1999; Bar-Matthews et al., 1998, 2003; Mayewski et al., 2004; Grant et al., 2012; Avnaim-Katav et al., 2017) than previously thought as shown in this study.

Although the A/P curve does not show correlations with periods of enhanced moisture (originated from the intensification of the monsoon system) documented in the sediments of unit II, the C/N maximum events are characterized by enhanced pollen concentrations, which is possibly due to better preservation during the accumulation of organic-rich sediments and thus likely a decrease in bottom water oxygen concentrations (Figs. 3 and 6; Langgut et al., 2011). Nevertheless, the *Artemisia*/Chenopodiaceae (A/C) ratio used as an indicator of effective moisture in arid and semi-arid regions (e.g., Liu et al., 1999) support unstable wetter conditions by displaying extreme fluctuations derived from increasing hydrological activity due to relatively enhanced rainfall from Mediterranean cyclones. The highest A/C values partly correspond to the C/N and TOC maxima in Unit II (Figs. 3 and 6). Consequently, we show in this study that the recorded high resolution climatic changes of the monsoon system and therefor the flow of the River Nile occasionally coincide with variations in the Mediterranean climate system.

Moreover, the single high peak in charcoal accumulation rates (CHAR) is observed at 3.27 kyr BP (Fig. 6 B). Charcoal data and the highest-magnitude of charcoal peaks are used to reconstruct fire activity which may be controlled naturally by local climate variability and vegetation characteristics or by anthropogenic influence (e.g., Power et al., 2010 and references therein). In our record the CHAR peak is observed parallel to the low C/N and TOC minima interpreted as dry periods and thus, may represent a fire event during an arid phase associated with the monsoonal and/or Mediterranean systems. Nevertheless, previous data suggests that fires in this region are biomass controlled; wildfires were least frequent when the climate was cold and dry and that they became more frequent and/or bigger during warmer and wetter climates which caused an increase in biomass availability (e.g., Turner et al., 2010). Consequently, the CHAR peak in core V-4, more likely represents landscape management by human activity. Humans can also modify natural fire regimes by starting and suppressing fires (accidentally or deliberately) through activities that lead to landscape fragmentation or changes in land cover (e.g., Archibald et al., 2009).

5.2. Paleoceanographic and climatic events during the mid-to Late Holocene in the eastern Mediterranean—implications for cultural change

It is well established that weakening of the monsoonal activity due to orbital changes since approximately 7.0 kyr BP has led to a gradual, regional aridification process along the entire latitudinal belt from Morocco to India (e.g., Rossignol-Strick, 1985; Hoelzmann et al., 2000; deMenocal et al., 2000; MacDonald, 2011). Nile delta sediments serve as ultimate archives for recording the catchment-wide effects of variability in the position of the Intertropical Convergence Zone (ITCZ) and associated precipitation and thus for reconstructions of northeast African climate (e.g. Fontugne et al., 1994; Cheddadi and Rossignol-Strick, 1995b; Almogi-Labin et al., 2009; Hennekam et al., 2014, 2015 and references therein). The current sedimentary sequence, accumulated at a site with a pronounced high sedimentation rate on the southeast Levantine shelf, may be one of the best records showing significant climate variability in NE Africa related to Nile discharge on multi-decadal time scales. The comparison of our data with other high-resolution sedimentary records, located further to the south and studied by Hennekam et al. (2014) shows quite similar trends between our data and geochemical proxies including the oxygen isotopes record of the planktonic foraminifer *Globigerinoides ruber* and bulk sediment Ba/Al and V/Al data (Fig. 7). These latter proxies are used as indicators for (export) productivity and redox conditions, respectively, and were associated with changes in Nile discharge (Hennekam et al., 2014).

5.2.1. The 4.2 kyr BP event as reflected by the benthic foraminiferal community

The relatively stable and arid period, between ~4.5 and ~3.8 cal kyr BP, is punctuated, by a maximum aridity event at 4.28 cal kyr BP (Fig. 7). Minimum TOC values, AP and A/C ratios indicate increasing aridification during this period in both regions may have been influenced by the monsoon and the Atlantic/Mediterranean climate systems. The foraminifera *Nonionella turgidus* occurs at its highest concentrations in the sediments accumulated during this event while, at the same time other species such as

Cribroelphidium poeyanum and *Valvulineria bradyana* declined in abundance (Fig. 4B). The appearance of the latter species, prior to this event can be connected to the relatively high TOC values since these species are known to prefer clayey substrates rich in organic matter (Jorissen, 1987; Avnaim-Katav et al., 2012, 2013, 2015, 2016b). The epifaunal to shallow-infaunal species *N. turgidus* shows an opportunistic lifestyle as it migrates rapidly to the uppermost sediment layer after environmental disturbance (Ernst et al., 2002), probably similar to its display during this abrupt arid event. Other evidence for an aridification events is the relatively sharp increase in $\delta^{15}N$ values up to 9.4‰ that follow the decrease in TOC. This high $\delta^{15}N$ values suggest nutrient stress (Francois and Altabet, 1994; Wada and Hattori, 1976) that could result from a decrease in river runoff. Alternatively, values exceeding 9‰ can imply denitrification probably in the sediments (Altabet et al., 1995), as bacterial denitrification processes taking place in oxygen-depleted zones, reducing the nitrate to gaseous nitrogen that causes a loss of oceanic nitrate (Jenkyns et al., 2001). Hence the consumption of nitrate from this pore water produces high isotopic signal in organic matter remains with values above 7‰ (e.g., Altabet et al., 1995; Somes et al., 2010). The presence of several benthic foraminiferal species in the record known to carry out full denitrification of nitrate to N_2, also supports our inference of denitrification taking place in the sediments (e.g., Piña-Ochoa et al., 2010). Species such as *V. bradyana* accumulate intracellular nitrate to millimolar concentrations, which they subsequently respire in the absence of oxygen (Piña-Ochoa et al., 2010). This species occurs in its highest concentrations in the sediments with high $\delta^{15}N$ values between ~4.4 and ~4.2 cal kyr BP (Fig. 4B).

High $\delta^{15}N$ values occur also at the ~3.6 and the 2.9 kyr BP transition suggesting drier climatic conditions, decrease in river runoff and denitrification at the marine system (Figs. 3 and 7). The high abundances of *Bulimina aculeata*, which have been shown to accumulate nitrate (Piña-Ochoa et al., 2010), during these transitions, especially at 2.9 kyr BP, also supports this inference (Fig. 3 and 4B).

The 4.2 kyr BP event occurred during the transition from Early Bronze IV to the Middle Bronze I (ca. 2200–1900 B.C. Levant archaeological periods, as summarized by Bar-Yosef and Garfinkel (2008)) at the end of a long period of gradual aridification (Bar-Matthews and Ayalon, 2011). Annual rainfall of ~350 mm in the southern Levantine highlands is estimated for this period based on oxygen isotope data derived from speleothems from Soreq Cave, Israel (Bar-Matthews and Ayalon, 2011). This arid event can tentatively be correlated with the well-studied 4.2 kyr BP drought event in south Asia, which has been associated with the termination of Indus Valley civilization (Weiss et al., 1993; MacDonald, 2011). It is one of the major, widespread and significant rapid climate change (RCC) events at 4200–3800 yr BP possibly caused by solar variability superimposed on long-term changes in insolation (e.g., Mayewski et al., 2004). This global scale event is evident from varied studies such as on speleothems in Italy (Drysdale et al., 2006) and the Eastern Mediterranean (e.g., Bar-Matthews et al., 1997; Bar-Matthews and Ayalon, 2011), low Dead Sea levels (Migowski et al., 2006), brine sediments from the Red Sea (Arz et al., 2006) as well as pelagic faunal response (e.g., Almogi-Labin et al., 2004), deep sea sediments in the Gulf of Oman (Cullen et al., 2000), ice cores from tropical Africa (Thompson et al., 2002). Staubwasser and Weiss (2006) refer to this event as a "Collapse as Adaptation to Rapid Climate Change" in northern Mesopotamia. They proposed that the synchronous changes observed among Early Bronze Age societies indicate a causal link with climate, i.e., reduced precipitation. This climatic change has led to the collapse of the politico-economic superstructures that were dependent upon cereal agriculture (Weiss et al., 1993; Staubwasser and Weiss, 2006). It seems, that the drought induced decline of ancient civilizations in Mesopotamia and south Asia is the consequence of altered extra tropical airflow during winter and a change in monsoon seasonality (Weiss et al., 1993). The impact of this change during this period includes the arid margins of the Levant, particularly the northern ones, where precipitation decline, settlement abandonment, population movements to more humid areas, and broader cultural changes have been identified (Weiss, 2014; Burke, 2017). Although the 4.2-ka event, is now recognized by many scientists to be the most prominent climatic episode of the middle to late Holocene (Kaniewski et al., 2018), it is important to emphasis that several archaeological records (e.g., alluvial stratigraphies) demonstrate other climatic trend (e.g. increased precipitation in the second half of the 5th millennium BC) associated with the foundation of new settlements in the northern Negev (e.g., Rosen, 2007).

5.2.2. Abrupt climate change at 3.58 and the transition to an unstable late Holocene climate (3.58–2.8 cal kyrBP)

A prominent transition from a stable and arid Mid-Late Holocene to an unstable late Holocene starting at ~3.6 cal kyr BP and culminating between 2.9 and 2.8 cal kyr BP (Fig. 7) is observed in core V-4. The changes in sedimentation rates and granulometry are coeval with general trends of Ba/Al and V/Al in core PS009PC, shifting to relatively higher values (Hennekam et al., 2014) during this transition (Fig. 7). These proxies, recorded by Hennekam et al. (2014) also show fluctuations and thus climatic instability during this period with simultaneous lower $\delta^{18}O_{G.\ ruber}$ values, higher Ba/Al and V/Al ratio, all attesting for increased periodic Nile discharge, increased (export) productivity and bottom water redox conditions.

This late Holocene climatic instability event was clearly documented by Schilman et al. (2001a) as demonstrating that humid phases occurred between 3.5 and 3.0 ka BP. However, their study featured a lower resolution compared to the higher resolution sedimentary archive reported in this study. Four distinct intervals in core V-4 with maximum positive excursions of C/N, TOC values and A/C and lower sedimentation rates, along with specific foraminiferal characteristics (high dominance of opportunistic foraminiferal species such as *A. tepida*) were interpreted as periods with wetter conditions and enhanced Nile River discharge at 3.5, 3.3, 3.2, and 3.0 kyr BP (chapter 5.1.1). These four intervals have close correspondence, though they do not entirely sync, with the inorganic geochemical proxies of Hennekam et al. (2014). Previous radiocarbon dating of paired foraminiferal and marine molluscan samples revealed age offsets between these materials, inferred to reflect greater reworking of foraminifera compared to the marine molluscs because of their lower effective density than the shell samples (Heier-Nielsen et al., 1995). This observation is more prominent in particular when the environment is characterized by high sedimentation rate (Heier-Nielsen et al., 1995). Consequently, The mass spectrometry measurements on planktonic foraminiferal used by Hennekam et al. (2014) compare to our radiocarbon dates of molluscs (mostly articulated) might produce these slight offsets in ^{14}C ages. In any event, macrofossil shell dates follow a smooth curve constituting a better, les problematic age model for dating the sediments.

Although a general transition to a more variable late Holocene climate has been recorded in places such as South Asia and correlated to increasing variability in Pacific Ocean SSTs (MacDonald, 2011). The abruptness and clarity of the climate change at 3.58 kyr BP in our record corresponds strikingly with the Minoan cataclysmic eruption of Santorini in the Aegean, often referred to as the "Thera eruption," which is dated ca. 1627–1600 BCE (3.577–3.550 kyr BP) based on radiocarbon determinations on olive wood branches buried during the eruption (Balter, 2006; Friedrich et al.,

2006). Studies reveal that high-latitude volcanic eruptions during historical times have led to Nile flood suppression (Oman et al., 2006; Manning et al., 2017). Volcanic aerosols affect temperatures and hydrology while altering precipitation and surface evaporation mainly by changing winds. Extratropical eruptions in the northern hemisphere increase aerosols cooling forming an energy sink which forces an anomalous Hadley circulation which shifts southward the intertropical convergence zone (ITCZ) away from that energy sink (Kang et al., 2008; Haywood et al., 2013). Consequently, a southward shift of northern hemisphere summer monsoon precipitation promotes drought in the northern parts of monsoon regions (e.g., Haywood et al., 2013; Liu et al., 2016).

Volcanic sulfate deposition associated with the Thera eruption exhibits no strong evidence (as yet) in global proxies such as in the tephra and trace element records of the Greenland ice cores (Coulter et al., 2012; Plunkett et al., 2017). Nonetheless, the significant impact of this event, both the immediate and prolonged, in disrupting the climate regime in the Levant seems likely.

Comparing merely the timing of the Thera eruption and our core data at 3.58 kyr BP (including: an increase in sedimentation rates and lower TOC values parallel a positive excursion in $\delta^{18}O_{G.\ ruber}$ values (recorded by Hennekam et al., 2014)) indicating a shift to an unstable late Holocene climate marked by fluctuation between wetter and drier conditions (Fig. 7). However, further research is needed in order to find direct evidence in core V-4 (e.g., identification of tephra shards) that would shed light whether this climate change is one of the impacts of the eruption of Santorini on the Levant and the greater eastern Mediterranean area.

6. Conclusions

Multi-proxy data including sedimentological, geochemical, organic matter stable isotope, foraminifera and pollen results from an unprecedentedly high sedimentation rate site in the SE Levantine shelf may be one of the paramount marine records yet presented of multi-decadal to centennial climate variability associated with Nile discharge during the Mid - to Late Holocene. Nile discharge was stable between 4.5 and ~3.6 cal kyr BP during arid conditions in the region that were interrupted by a maximum peak in aridity at 4.28 kyr BP. This climate deterioration in the Levant appears to accord with the well-studied drought event that also impacted the arid margins of southwest and south Asia around 4.2 kyr BP.

This prominent event recorded at 4.28, and the transitional periods at ~3.6 and at 2.9 kyr BP are characterized by simultaneous high $\delta^{15}N$ values and low total organic carbon (TOC) suggesting drier climatic conditions, decrease in Nile river runoff and nutrient supply to the marine system (i.e., Nile discharge) and possible denitrification at the marine system evidenced by the increased concentrations of foraminifera capable of performing denitrification (e.g., *Valvulineria bradyana*).

The climate during the late Holocene, between ~3.6 and 2.8 cal kyr BP, was unstable and was probably characterized by significant fluctuations between relatively drier and wetter conditions than today. The arid periods are characterized by low TOC, C/N ratio and high $\delta^{15}N$ values suggested nutrient stress as result of lower river discharge.

During the wetter phases, at 3.5, 3.3, 3.2, and 3.0 kyr BP, discharge of the Nile notably increased the transportation of terrestrial organic matter and nutrients to the sea-water impacting the foraminiferal assemblages. The climatic shift at 3.58 kyr BP may have been influenced by the Thera eruption. This finding may reveal, therefore, that this well-known volcanic eruption had a wide range climatic effect that reached much of the ancient Near East and Egypt.

Acknowledgments

We gratefully acknowledge Maarten Blaauw for assistance with Bacon. The contribution to the picking process of foraminifera of Auri Menirom of Ben Gurion University is highly appreciated. Thanks are due to Lauren N. Brown for preparation of the samples for ^{14}C dating at the Keck Carbon Cycle AMS Facility (Irvine, CA). We thank Yael Jacoby-Glass and Guy Tau from the GSI for the grain size analysis.

Appendix A. Supplementary data

Supplementary data to this article can be found online at https://doi.org/10.1016/j.quascirev.2018.12.001.

References

Adamson, D.A., Gasse, F., Street, F.A., Williams, M.A.J., 1980. Late quaternary history of the Nile. Nature 288, 50–55.
Almagor, G., Gill, D., Golik, A., 1998. Artificial Islands Project; Geotechnical Tests of Vibracores . Geological Survey Report GSI/28/1998 (In Hebrew, English abstract).
Almagor, G., Gill, D., Perath, I., 2000. Marine sand resources offshore Israel. Mar. Georesour. Geotechnol. 18, 1–42.
Almogi-Labin, A., Bar-Matthews, M., Ayalon, A., 2004. Climate variability in the Levant and northeast Africa during the Late Quaternary based on marine and land records. In: Naama, Goren-Inbar, John, D. (Eds.), Human Paleoecology in the Levantine Corridor. Oxbow Press, Speth, Oxford, pp. 117–134.
Almogi-Labin, A., Bar-Matthews, M., Shriki, D., Kolosovsky, E., Paterne, M., Schilman, B., Ayalon, A., Aizenshtat, Z., Matthews, A., 2009. Climatic variability during the last ~90 ka of the southern and northern Levantine Basin as evident from marine records and speleothems. Quat. Sci. Rev. 28, 2882–2896.
Almogi-Labin, A., Calvo, R., Elyashiv, H., Amit, R., Harlavan, Y., Herut, H., 2012. Sediment Characterization of the Israeli Mediterranean Shelf. GSI Report GSI/27/2012 and IOLR Report H68/2012, p. 38.
Altabet, M.A., Francois, R., Murray, D.W., Prell, W.L., 1995. Climate-related variations in denitrification in the Arabian sea from sediment n-15/n-14 ratios. Nature 373 (6514), 506–509.
Archibald, S., Roy, D.P., van Wilgen, B., Scholes, R.J., 2009. What limits fire? An examination of drivers of burnt area in Southern Africa. Global Change Biol. 15, 613–630.
Arz, H.W., Lamy, F., Pätzold, J., 2006. A pronounced dry event recorded around 4.2 kyr in brine sediments from the Northern Red Sea. Quat. Res. 66, 432–441.
Avital, A., 2002. Sedimentological and Micropaleontological Characterization of Late Quaternary Sediments from Boreholes off Ashqelon. MSc thesis. Ben Gurion University of the Negev, Beer Sheva (in Hebrew, English abstract).
Avnaim-Katav, S., Almogi-Labin, A., Sandler, A., Sivan, D., Porat, N., Matmon, A., 2012. The chronostratigraphy of a Quaternary sequence at the distal part of the Nile Littoral cell, Haifa Bay, Israel. J. Quat. Sci. 27, 675–686.
Avnaim-Katav, S., Almogi-Labin, A., Sandler, A., Sivan, D., 2013. Benthic foraminifera as paleoenvironmental indicators during the lastmillion years in the eastern Mediterranean inner shelf. Palaeogeogr. Palaeoclimatol. Palaeoecol. 386, 512–530.
Avnaim-Katav, S., Hyams-Kaphzan, O., Milker, Y., Almogi-Labin, A., 2015. Bathymetric zonation of modern shelf benthic foraminifera in the Levantine Basin, eastern Mediterranean Sea. J. Sea Res. 99, 97–106.
Avnaim-Katav, S., Agnon, A., Sivan, D., Almogi-Labin, A., 2016a. Calcareous assemblages of the southeastern Mediterranean low-tide estuaries—seasonal dynamics and paleoenvironmental implications. J. Sea Res. 108, 30–49.
Avnaim-Katav, S., Milker, Y., Schmiedl, G., Sivan, D., Hyams-Kaphzan, O., Sandler, A., Almogi-Labin, A., 2016b. Impact of eustatic and tectonic processes on the southeastern Mediterranean shelf: quantitative reconstructions using a foraminiferal transfer function. Mar. Geol. 376, 26–38.
Avnaim-Katav, S., Almogi-Labin, A., Agnon, A., Porat, N., Sivan, D., 2017. Mid-to late-Holocene hydrological events and human induced environmental changes reflected in a southeastern Mediterranean fluvial archive. Palaeogeogr. Palaeoclimatol. Palaeoecol. 468, 263–275.
Balter, M., 2006. New carbon dates support revised history of ancient mediterranean. Science 312, 508–509.
Bar-Matthews, M., Ayalon, A., Kaufman, A., 1997. Late Quaternary paleoclimate in the eastern Mediterranean region from stable isotope analysis of speleothems at Soreq Cave, Israel. Quat. Res. 47, 155–168.
Bar-Matthews, M., Ayalon, A., Kaufman, A., 1998. Middle to late Holocene (6500 years period) paleoclimate in the eastern Mediterranean region from stable isotopic composition of speleothems from Soreq Cave, Israel. In: Issar, A.S., Brown, N. (Eds.), Water, Environment and Society in Times of Climate Change. Kluwer Academic Publishers, pp. 203–214.
Bar-Matthews, M., Ayalon, A., Gilmour, M., Matthews, A., Hawkesworth, C.J., 2003. Sea-land oxygen isotopic relationships from planktonic foraminifera and speleothems in the Eastern Mediterranean region and their implication for

paleorainfall during interglacial intervals. Geochem. Cosmochim. Acta 67, 3181–3199.
Bar-Matthews, M., Ayalon, A., 2011. Mid- Holocene climate variations revealed by highresolution speleothem records from Soreq Cave, Israel and their correlation with cultural changes. Holocene 21, 163–171.
Bar-Yosef, O., Garfinkel, Y., 2008. The Prehistory of Israel, Human Cultures before Writing. Ariel Publishing House, Museum of Yarmukian Culture at Sha'ar Hagolan, Jerusalem, p. 351.
Beug, H.J., 1975. Changes of climate and vegetation belts in the mountains of Mediterranean Europe during the Holocene. Bull. Geol. 19, 101–110.
Beug, H.J., 2004. Leitfaden der Pollenbestimmung: für Mitteleuropa und angrenzende Gebiete. Pfeil, München.
Bianchi, G.G., McCave, N., 1999. Holocene periodicity in North Atlantic climate and deep-ocean flow south of Iceland. Nature 397, 515–517.
Blaauw, M., Christen, A., 2011. Flexible paleoclimate age-depth models using an autoregressive gamma process. Bayesian Anal. 6, 457–474.
Box, M.R., Krom, M.D., Cliff, R.A., Bar-Matthews, M., Almogi-Labin, A., Ayalon, A., Paterne, M., 2011. Response of the Nile and its catchment to millennial-scale climatic change since the LGM from Sr isotopes and major elements of East Mediterranean sediments. Quat. Sci. Rev. 30, 431–442.
Burke, A.A., 2017. Amorites, climate change and the negotiation of identity at the end of the third millennium B.C. In: Höflmayer, F. (Ed.), The Late Third Millennium in the Ancient Near East: Chronology, C14, and Climate Change. Oriental Institute, Chicago, pp. 261–308.
Buzas, M.A., Gibson, T.G., 1969. Species diversity: benthonic foraminifera in western north atlantic. Science 163, 72–75.
Cheddadi, R., Rossignol-Strick, M., 1995a. Eastern Mediterranean Quaternary paleoclimates from pollen and isotope records of marine cores in the Nile cone area. Paleoceanography 10, 291–300.
Cheddadi, R., Rossignol-Strick, M., 1995b. Improved preservation of organic matter and pollen in Eastern Mediterranean saproples. Paleoceanography 10, 301–309.
Cimerman, F., Langer, M.R., 1991. Mediterranean Foraminifera. Academia Scientarium et Aritium Slovenica, Dela, Opera 30, Classis IV: Historia Naturalis (118 p., 93 pl.).
Coulter, S.E., Pilcher, J.R., Plunkett, G., Baillie, M., Hall, V.A., Steffensen, J.P., Vinther, B.M., Clausen, H.B., Johnsen, S.J., 2012. Holocene tephras highlight complexity of volcanic signals in Greenland ice cores. J. Geophys. Res.: Atmosphere 117, D21303.
Cullen, H.M., deMenocal, P.B., Hemming, S., Hemming, G., Brown, F.H., Guilderson, T., Sirocko, F., 2000. Climate change and the collapse of the Akkadian empire: evidence from the deep sea. Geology 28, 379–382.
Drysdale, R., Zanchetta, G., Hellstrom, J., Maas, R., Fallick, A., Pickett, M., Cartwright, I., Piccini, L., 2006. Late Holocene drought responsible for the collapse of Old World civilizations is recorded in an Italian cave flowstone. Geology 34, 101–104.
Enzel, Y., Bookman (Ken-Tor), R., Sharon, D., Gvirtzman, H., Dayan, U., Ziv, B., Stein, M., 2003. Late Holocene climates of the Near East deduced from Dead Sea level variations and regional winter rainfall. Quat. Res. 60, 263–273.
Enzel, Y., Amit, R., Dayan, U., Crouvi, O., Kahana, R., Ziv, B., et al., 2008. The climatic and physiographic controls of the eastern Mediterranean over the late Pleistocene climates in the southern Levant and its neighboring deserts. Global Planet. Change 60, 165–192.
Ernst, S., Duijnstee, I., van der Zwaan, B., 2002. The dynamics of the benthic foraminiferal microhabitat: recovery after experimental disturbance. Mar. Micropaleontol. 46, 343–361.
Faegri, K., Iversen, J., 1992. Textbook of Pollen Analysis, fourth ed. John Wiley and Sons, Sons, London.
Fisher, P., Aumann, C., Chia, K., O'Halloran, N., Chandra, S., 2017. Adequacy of laser diffraction for soil particle size analysis. PloS One 12 e0176510.
Fisher, R.A., Corbet, A.S., Williams, C.B., 1943. The relation between the number of species and the number of individuals in a random sample of an animal population. J. Anim. Ecol. 12, 42–58.
Fleitmann, D., Burns, S.J., Mangini, A., Mudelsee, M., Kramers, J., Villa, I., Neff, U., Al-Subbary, A.A., Buettner, A., Hippler, D., Matter, A., 2007. Holocene ITCZ and Indian monsoon dynamics recorded in stalagmites from Oman and Yemen (Socotra). Quat. Sci. Rev. 26, 170–188.
Francois, R., Altabet, M.A., 1994. Glacial to interglacial changes in surface nitrate utilization in the Indian sector of the Southern Ocean as recorded by sediment $d^{15}N$. Paleoceanography 7 (5), 589–606.
Friedrich, W.L., Kroner, B., Friedrich, M., Heinemeier, J., Pfeiffer, T., Talamo, S., 2006. Santorini eruption radiocarbon dated to 1627–1600 B.C. Science 312, 548.
Fontugne, M.R., Arnold, M., Labeyrie, L., Paterne, M., Calvert, S.E., Duplessy, J.C., 1994. Paleoenvironment, sapropel chronology and Nile River discharge during the last 20,000 years as indicated by deep-sea sediment records in the eastern Mediterranean. In: Bar-Yosef, O., Kra, R.S. (Eds.), Late Quaternary Chronology and Paleoclimates of the Eastern Mediterranean. Radiocarbon, Tucson, pp. 75–88.
Golik, A., 1993. Indirect evidence for sediment transport on the continental shelf off Israel. Geo Mar. Lett. 13, 159–164.
Grant, K.M., Rohling, E.J., Bar-Matthews, M., Ayalon, A., Medina-Elizalde, M., Bronk Ramsey, C., Satow, C., Roberts, A.P., 2012. Rapid coupling between ice volume and polar temperature over the past 150 kyr. Nature 491, 744–747.
Grimm, E., 1990. TILIA and TILIA.GRAPH: PC spreadsheets and graphics software for pollen data. INQUA Comm. Stud. Holocene Working Group on Data-Handling Methods. Newslettter 4, 5–7.
Hamann, Y., Ehrmann, W., Schmiedl, G., Kuhnt, T., 2009. Modern and late Quaternary clay mineral distribution in the area of the SE Mediterranean Sea. Quat. Res. 71, 453–464.
Haywood, J.M., Jones, A., Bellouin, N., Stephenson, D., 2013. Asymmetric forcing from stratospheric aerosols impacts Sahelian rainfall. Nat. Clim. Change 3, 660–665.
Hedges, J.I., Clark, W.A., Quay, P.D., Richey, J.E., Devol, A.H., Santos, U.D., 1986. Compositions and fluxes of particulate organic material in the Amazon river. Limnol. Oceanogr. 31 (4), 717–738.
Heier-Nielsen, S., Conradsen, K., Heinemeier, J., Knudsen, K.L., Nielsen, H.L., Rud, N., Sveinbjörnsdóttir, Á.E., 1995. Radiocarbon dating of shells and foraminifera from the Skagen core, Denmark: evidence of reworking. Radiocarbon 37 (2), 119–130.
Hennekam, R., Jilbert, T., Schnetger, B., de Lange, G.J., 2014. Solar forcing of Nile discharge and sapropel S1 formation in the early to middle Holocene eastern Mediterranean. Paleoceanography 29, 2013PA002553.
Hennekam, R., Donders, T.H., Zwiep, K., de Lange, G.J., 2015. Integral view of Holocene precipitation and vegetation changes in the Nile catchment area as inferred from its delta sediments. Quat. Sci. Rev. 130, 189–199.
Hoelzmann, P., Kruse, H.-J., Rottinger, F., 2000. Precipitation estimates for the eastern Saharan palaeomonsoon based on a water balance model of the West Nubian Palaeolake Basin. Global Planet. Change 26, 105–120.
Hughen, K.A., Baillie, M.G.L., Bard, E., Bayliss, A., Beck, J.W., Bertrand, C.J.H., Blackwell, P.G., Buck, C.E., Burr, G.S., Cutler, K.B., Damon, P.E., Edwards, R.L., Fairbanks, R.G., Friedrich, M., Guilderson, T.P., Kromer, B., McCormac, F.G., Manning, S.W., Bronk Ramsey, C., Reimer, P.J., Reimer, R.W., Remmele, S., Southon, J.R., Stuiver, M., Talamo, S., Taylor, F.W., van der Plicht, J., Weyhenmeyer, C.E., 2004. Marine 04 Marine radiocarbon age calibration, 26 - 0 ka BP. Radiocarbon 46, 1059–1086.
Hyams-Kaphzan, O., Almogi-Labin, A., Sivan, D., Benjamini, C., 2008. Benthic foraminifera assemblage change along the southeastern Mediterranean inner shelf due to fall-off of Nile-derived siliciclastics. Neues Jahrbuch Geol. Palaontol. Abhand. 248, 315–344.
Hyams-Kaphzan, O., Almogi-Labin, A., Benjamini, C., Herut, B., 2009. Natural oligotrophy vs. pollution-induced eutrophy on the SE Mediterranean shallow shelf (Israel): environmental parameters and benthic foraminifera. Mar. Pollut. Bull. 58, 1888–1902.
Jenkyns, H.C., Grocke, D.R., Hesselbo, S.P., 2001. Nitrogen isotope evidence for water mass denitrification during the early Toarcian (Jurassic) oceanic anoxic event. Paleoceanography 16 (6), 593–603.
Jorissen, F.J., 1987. The distribution of benthic foraminifera in the Adriatic Sea. Mar. Micropaleontol. 12, 21–48.
Jorissen, F.J., 1988. Benthic foraminifera from the Adriatic Sea: principles of phenotypic variation. Utrecht Micropaleontol. Bull. 37–174.
Kang, S.M., Held, I.M., Frierson, D.M.W., Zhao, M., 2008. The response of the ITCZ to extratropical thermal forcing: idealized slab-ocean experiments with a GCM. J. Clim. 21, 3521–3532.
Kaniewski, D., Marriner, N., Cheddadi, R., Joel, G., Van Campo, E., 2018. The 4.2 ka BP event in the Levant. Clim. Past 14, 1529–1542.
Kohn, M.J., 2010. Carbon isotope compositions of terrestrial C3 plants as indicators of (paleo)ecology and (paleo)climate. Proc. Natl. Acad. Sci U. S. A. 107, 19691–19695.
Krom, M.D., Cliff, R.A., Eijsink, L.M., Herut, B., Chester, R., 1999. The characterization of Saharan dusts and Nile particulate matter in surface sediments from the Levantine basin using Sr isotopes. Mar. Geol. 155, 319–330.
Krom, M.D., Stanley, J.D., Cliff, P.A., Woodward, J.C., 2002. Nile River sediment fluctuations over the past 7,000 yr and their key role in sapropel development. Geology 30, 71–74.
Langgut, D., Almogi-Labin, A., Bar-Matthews, Weinstein-Evron, M., 2011. Vegetation and climate changes in the South Eastern Mediterranean during the Last Glacial-Interglacial cycle (86 ka): new marine pollen record. Quat. Sci. Rev. 30, 3960–3972.
Levin, L.A., Gage, J.D., 1998. Relationships between oxygen, organic matter and the diversity of bathyal macrofauna. Deep-Sea Res. 45, 129–163.
Liu, H.Y., Cui, H.T., Pott, R., Speier, M., 1999. The surface pollen of the woodland-steppe ecotone in southeastern Inner Mongolia, China. Rev. Palaeobot. Palynol. 105, 237–250.
Liu, F., Chai, J., Wang, B., Liu, J., Zhang, X., Wang, Z., 2016. Global monsoon precipitation responses to large volcanic eruptions. Sci. Rep. 6, 24331. https://doi.org/10.1038/srep24331.
Magana, A.L., Southon, J.R., Kennett, J.P., Roark, E.B., Sarnthein, M., Stott, L.D., 2010. Resolving the cause of large differences between deglacial benthic foraminifera radiocarbon measurements in Santa Barbara Basin. Paleoceanography 25, PA4102. https://doi.org/10.1029/2010PA002011.
MacDonald, G., 2011. Potential influence of the Pacific Ocean on the Indian summer monsoon and harappan decline. Quat. Int. 229, 140–148.
Malanotte-Rizzoli, P., Robinson, A.R., Roether, W., Manca, B., Bergamasco, A., Brenner, S., Civitarese, G., Georgopoulos, D., Haley, P.J., Kioroglou, S., Kontoyannis, H., Kress, N., Latif, M.A., Leslie, W.G., Ozsoy, E., Ribera d'Alcala, M., Salihoglu, I., Sansone, E., Theocharis, A., 1996. Experiment in Eastern Mediterranean probes origin of deep water. Eos 77, 305.
Manning, J.G., Ludlow, F., Stine, A.R., Boos, W.R., Sigl, M., Marlon, J.R., 2017. Volcanic suppression of Nile summer flooding triggers revolt and constrains interstate conflict in ancient Egypt. Nat. Commun. 8 (1–9), 900.
Mayewski, P.A., Rohling, E.E., Stager, J.C., Karlen, W., Maascha, K.A., Meekler, L.D.,

Meyerson, E.A., Gasse, F., van Kreveld, S., Holmgren, K.U., 2004. Holocene climate variability. Quat. Res. 62, 243–255.
McGarry, S., Bar-Matthews, M., Matthews, A., Vaks, A., Schilman, B., Ayalon, A., 2004. Constraints on hydrological and paleotemperature variations in the eastern Mediterranean region in the last 140ka given by the δD values of speleothem fluid inclusions. Quat. Sci. Rev. 23, 919–934.
Meyers, P.A., Teranes, J.L., 2001. Sediment Organic Matter, Tracking Environmental Change Using Lake Sediments Physical and Geochemical Methods. Chapter 9.
Migowski, C., Stein, M., Prasad, S., Negendank, J.F.W., Agnon, A., 2006. Holocene climate variability and cultural evolution in the Near East from the Dead Sea sedimentary record. Quat. Res. 66, 421–431.
Miller, B.A., Schaetzl, R.J., 2012. Precision of soil particle size analysis using laser diffractometry. Soil Sci. Soc. Am. J. 76, 1719–1727.
Mohamed, Y.A., van den Hurk, B.J.J.M., Savenije, H.H.G., Bastiaanssen, W.G.M., 2005. Hydroclimatology of the Nile: results from a regional climate model. Hydrol. Earth Syst. Sci. 9, 263–278.
Mojtahid, M., Manceau, R., Schiebel, R., Hennekam, R., De Lange, G.J., 2015. Thirteen thousand years of southeastern Mediterranean climate variability inferred from an integrative planktic foraminiferal-based approach. Paleoceanography 30, 2014PA002705.
Moore, P.D., Webb, J.A., Collinson, M.E., 1991. Pollen Analysis, second ed. Blackwell Scientific Publications, Oxford.
Murray, J.W., 1991. Ecology and Palaeoecology of Benthic Foraminifera. Longman, Harlow, p. 397.
Oman, L., Robock, A., Stenchikov, G.L., Thordarson, T., 2006. High-latitude eruptions cast shadow over the African monsoon and the flow of the Nile. Geophys. Res. Lett. 33, L18711. https://doi.org/10.1029/2006GL027665.
Overpeck, J., Anderson, D., Trumbore, S., Prell, W., 1996. The southwest Indian Monsoon over the last 18000 years. Clim. Dynam. 12 (3), 213–225.
Piña-Ochoa, E., Høgslund, S., Geslin, E., Cedhagen, T., Revsbech, N.P., Lars Nielsen, P., Schweizer, M., Jorissen, F., Rysgaard, S., Risgaard-Petersen, N., 2010. Widespread occurrence of nitrate storage and denitrification among Foraminifera and Gromiida. Proc. Natl. Acad. Sci. U. S. A. 107, 1148–1153.
Pinardi, N., Masetti, E., 2000. Variability of the large scale general circulation of the Mediterranean Sea from observations and modelling: a review. Palaeogeogr. Palaeoclimatol. Palaeoecol. 158, 153–174.
Plunkett, G., Nick, J.G., Pearce, J.R., McConell, J.R., Pilcher, M.S., Hongli, Z., 2017. Trace element analysis of Late Holocene tephras from Greenland ice cores. Quat. Newsl. 143, 10–20.
Porat, N., Avital, A., Frechen, M., Almogi-Labin, A., 2003. Chronology of upper Quaternary offshore successions from the southeastern Mediterranean Sea. Quat. Sci. Rev. 22, 1191–1199.
Porat, N., Sivan, D., Zviely, D., 2008. Late Holocene embayment and sedimentological infill processes in Haifa Bay, SE mediterranean. Isr. J. Earth Sci. 57, 21–23.
Power, M.J., Marlon, J.R., Bartlein, P.J., Harrison, S.P., 2010. Fire history and the Global Charcoal Database: a new tool for hypothesis testing and data exploration. Palaeogeogr. Palaeoclimatol. Palaeoecol. 291, 52–59.
Reimer, P.J., Bard, E., Bayliss, A., Beck, J.W., Blackwell, P.G., Bronk Ramsey, C., Grootes, P.M., Guilderson, T.P., Haflidason, H., Hajdas, I., HattŽ, C., Heaton, T.J., Hoffmann, D.L., Hogg, A.G., Hughen, K.A., Kaiser, K.F., Kromer, B., Manning, S.W., Niu, M., Reimer, R.W., Richards, D.A., Scott, E.M., Southon, J.R., Staff, R.A., Turney, C.S.M., van der Plicht, J., 2013. IntCal13 and Marine13 radiocarbon age calibration curves 0-50,000 Years cal BP. Radiocarbon 55 (4).
Reille, M., 1995. Pollen et Spores d'Europe et d'Afrique du Nord. supplement 1. Laboratoire de Botanique Historique et Palynologie, Marseille.
Reille, M., 1998. Pollen et Spores d'Europe et d'Afrique du Nord. supplement 2. Laboratoire de Botanique Historique et Palynologie, Marseille.
Reille, M., 1999. Pollen et Spores d'Europe et d'Afrique du Nord, II edition. Laboratoirede Botanique Historique et Palynologie, Marseille.
Rohling, E.J., 1994. Review and new aspects concerning the formation of Mediterranean sapropels. Mar. Geol. 122, 1–28.
Rosen, A.M., 2007. Civilizing Climate, Social Responses to Climate Change in the Ancient Near East. Altamira Press, New York.
Rossignol-Strick, M., Nesteroff, W., Olive, P., Vergnaud-Grazzini, C., 1982. After the deluge: mediterranean stagnation and sapropel formation. Nature 295, 105–110.
Rossignol-Strick, M., 1983. African monsoon an immediate climate response to orbital insolation. Nature 304, 46–49.
Rossignol-Strick, M., 1985. Mediterranean Quaternary sapropels, an immediate response of the African monsoon to variation of insolation. Palaeogeogr. Palaeoclimatol. Palaeoecol. 49, 237–263.
Rossignol-Strick, M., Planchais, N., 1989. Climate patterns revealed by pollen and oxygen isotope records of a Tyrrhenian Sea core. Nature 342, 413–416.
Said, R., 1993. The River Nile: Geology, Hydrology and Utilization. Pergamon Press, Oxford.
Sandler, A., Herut, B., 2000. Composition of clays along the continental shelf off Israel: contribution of the Nile versus local sources. Mar. Geol. 167, 339–354.
Schilman, B., Bar-Matthews, M., Almogi-Labin, A., Luz, B., 2001a. Global climate instability reflected by Eastern Mediterranean marine records during the late Holocene. Palaeogeogr. Palaeoclimatol. Palaeoecol. 176, 157–176.
Schilman, B., Almogi-Labin, A., Bar-Matthews, M., Labeyrie, L., Paterne, M., Luz, B., 2001b. Long- and short-term carbon fluctuations in the Eastern Mediterranean during the late Holocene. Geology 29, 1099–1102.
Schmidt, M.W.I., Noack, A.G., 2000. Black carbon in soils and sediments: analysis, distribution, implications, and current challenges. Global Biogeochem. Cycles 14, 777–793.
Sgarrella, F., Moncharmont-Zei, M., 1993. Benthic foraminifera of the Gulf of Naples (Italy): systematics and autoecology. Boll. Soc. Paleontol. Ital. 32, 145–264.
Sivan, D., Wdowinsky, S., Lambeck, K., Galili, E., Raban, A., 2001. Holocene sea-level changes along the Mediterranean coast of Israel, based on archaeological observations and numerical model. Palaeogeogr. Palaeoclimatol. Palaeoecol. 167, 101–117.
Sollins, P., Swanston, C., Kleber, M., Filley, T., Kramer, M., Crow, S., Caldwell, B.A., Lajtha, K., Bowden, R., 2006. Organic C and N stabilization in a forest soil: evidence from sequential density fractionation. Soil Biol. Biochem. 38, 3313–3324.
Somes, C.J., Schmittner, A., Galbraith, E.D., Lehmann, M.F., Altabet, M.A., Montoya, J.P., Letelier, R.M., Mix, A.C., Bourbonnais, A., Eby, M., 2010. Simulating the global distribution of nitrogen isotopes in the ocean. Global Biogeochem. Cycles 24, GB4019. https://doi.org/10.1029/2009GB003767.
Staubwasser, M., Weiss, H., 2006. Holocene climate and cultural evolution in late prehistoric–early historic West Asia–Introduction. Special Issue. Quat. Res. 66, 372–387.
Stockmarr, J., 1971. Tablets with sporcs used in absolute pollen analysis. Pollen Spores 13, 615–621.
Stuiver, M., Reimer, P.J., 1993. Extended 14C database and revised CALIB radiocarbon calibration program. Radiocarbon 35, 215–230.
Tadir, R., Benjamini, C., Almogi-Labin, A., Hyams-Kaphzan, O., 2017. Temporal trends in live foraminiferal assemblages near a pollution outfall on the Levant shelf. Mar. Pollut. Bull. 117 (1–2), 50–60. https://doi.org/10.1016/j.marpolbul.2016.12.045.
Tapiero, I., 2002. High-resolution Paleoecologic and Paleoclimatic Changes of the Holocene, Based on Benthic Foraminifera and Sediments from the Mediterranean Inner Shelf, Israel (MSc Thesis). Ben-Gurion University of the Negev, Beer Sheva, Israel, p. 130 (In Hebrew, English abstract).
Thompson, L.G., Mosley-Thompson, E., Davis, M.E., Henderson, K.A., Brecher, H.H., Zagorodnov, V.S., Mashiotta, T.A., Lin, P.N., Mikhalenko, V.N., Hardy, D.R., Beer, J., 2002. Kilimanjaro ice core records: evidence of Holocene climate change in tropical Africa. Science 298, 589–593.
Thunell, R.C., Williams, D.F., 1989. Glacial–Holocene salinity changes in the Mediterranean Sea: hydrographic and depositional effects. Nature 338, 493–496.
Turner, R., Roberts, N., Eastwood, W.J., Jenkins, E., Rosen, A., 2010. Fire, climate and the origins of agriculture: micro-charcoal records of biomass burning during the last glacial–interglacial transition in Southwest Asia. J. Quat. Sci. 25, 371–386.
Twichell, S.C., Meyers, P.A., Diester-Haass, L., 2002. Significance of high C/N ratios in organic-carbon-rich Neogene sediments under the Benguela Current upwelling system. Org. Geochem. 33 (7), 715–722.
Wada, E., Hattori, A., 1976. Natural abundance of ^{15}N in particular organic matter in North Pacific Ocean. Geochem. Cosmochim. Acta v. 40, 249–251.
Weiss, H., Courty, M.A., Wetterstrom, W., Guichard, F., Senior, L., Meadow, R., Curnow, A., 1993. The genesis and collapse of 3rd millennium north Mesopotamian civilization. Science 261, 995–1004.
Weiss, H., 2014. The northern levant during the intermediate Bronze age: altered trajectories. In: Steiner, M.L., Killebrew, A.E. (Eds.), The Oxford Handbook of the Archaeology of the Levant (C. 8000–332 BCE). Oxford University Press, Oxford, pp. 367–387.
Whitlock, C., Larsen, C., 2001. Charcoal as a fire proxy. In: Smol, J.P., Birks, H.J.B., Last, W.M. (Eds.), Tracking Environmental Change Using Lake Sediments. Terrestrial, Algal, & Siliceous Indicators, vol. 3. Kluwer Academic Publishers, Dordrecht, pp. 75–97.
Ziv, B., Saaroni, H., Alpert, P., 2004. The factors governing the summer regime of the eastern Mediterranean. Int. J. Climatol.: J. Roy. Meteorol. Soc. 24 (14), 1859–1871.
Ziv, B., Dayan, U., Kushnir, Y., Roth, C., Enzel, Y., 2006. Regional and global atmospheric patterns governing rainfall in the southern Levant. Int. J. Climatol. 26, 55–73.
Zviely, D., Kit, E., Klein, M., 2007. Longshore sand transport estimates along the Mediterranean coast of Israel in the Holocene. Mar. Geol. 238, 61–73.